Title

Targeting the non-coding genome and temozolomide signature enables CRISPR-mediated glioma oncolysis.

Journal

Cell Reports, 42(11)

Authors

Tan, I-Li

Perez, Alexendar

Lew, Rachel

et al.

Publication Date

2023-11-28

DOI

10.1016/j.celrep.2023.113339

Peer reviewed

HHS Public Access

Author manuscript

Cell Rep. Author manuscript; available in PMC 2023 December 17.

Published in final edited form as:

Cell Rep. 2023 November 28; 42(11): 113339. doi:10.1016/j.celrep.2023.113339.

Targeting the non-coding genome and temozolomide signature enables CRISPR-mediated glioma oncolysis

I-Li Tan[1,2,9,11], **Alexendar R. Perez**[3,4,11], **Rachel J. Lew**[1], **Xiaoyu Sun**[4], **Alisha Baldwin**[1,2], **Yong K. Zhu**[1,2], **Mihir M. Shah**[1,5], **Mitchel S. Berger**[6], **Jennifer A. Doudna**[1,2,5,7], **Christof Fellmann**[1,5,8,10,12,*]

[1]Gladstone Institute of Data Science and Biotechnology, Gladstone Institutes, San Francisco, CA 94158, USA

[2]Innovative Genomics Institute, University of California, Berkeley, Berkeley, CA 94720, USA

[3]Department of Anesthesia and Perioperative Care, University of California, San Francisco, San Francisco, CA 94131, USA

[4]Silico Therapeutics, San Francisco, CA 94131, USA

[5]Department of Molecular and Cell Biology, University of California, Berkeley, Berkeley, CA 94720, USA

[6]Department of Neurological Surgery, University of California, San Francisco, San Francisco, CA 94131, USA

[7]Howard Hughes Medical Institute, University of California, Berkeley, Berkeley, CA 94720, USA

[8]Department of Cellular and Molecular Pharmacology, University of California, San Francisco, San Francisco, CA 94158, USA

[9]Present address: Evercrisp Biosciences, Berkeley, CA 94720, USA

[10]Present address: CRISPR Therapeutics, San Francisco, CA 94158, USA

[11]These authors contributed equally

[12]Lead contact

*Correspondence: christof.fellmann@gladstone.ucsf.edu.

AUTHOR CONTRIBUTIONS

I.T. and A.R.P. contributed equally to this work. C.F. conceived the project. I.T., A.R.P., and C.F. planned, carried out, and analyzed experiments. R.J.L., X.S., A.B., Y.K.Z., and M.M.S. performed experiments and provided technical support. M.S.B., J.A.D., and C.F. provided conceptual support. I.T., A.R.P., and C.F. wrote the manuscript with input from M.S.B. and J.A.D. All authors reviewed the final manuscript.

DECLARATION OF INTERESTS

The Regents of the University of California and the J. David Gladstone Institutes have filed a patent related to this work, on which C.F. is listed as inventor. Silico Therapeutics has filed a patent related to this work, on which A.R.P. and X.S. are listed as inventors. J.A.D. is a co-founder of Caribou Biosciences, Editas Medicine, Intellia Therapeutics, Scribe Therapeutics, and Mammoth Biosciences. J.A.D. is a scientific advisory board member of Caribou Biosciences, Intellia Therapeutics, eFFECTOR Therapeutics, Scribe Therapeutics, Synthego, Metagenomi, Mammoth Biosciences, and Inari. J.A.D. is a member of the board of directors at Driver and Johnson & Johnson. C.F. is a co-founder of Mirimus, Inc.

SUPPLEMENTAL INFORMATION

Supplemental information can be found online at https://doi.org/10.1016/j.celrep.2023.113339.

SUMMARY

Glioblastoma (GBM) is the most common lethal primary brain cancer in adults. Despite treatment regimens including surgical resection, radiotherapy, and temozolomide (TMZ) chemotherapy, growth of residual tumor leads to therapy resistance and death. At recurrence, a quarter to a third of all gliomas have hypermutated genomes, with mutational burdens orders of magnitude greater than in normal tissue. Here, we quantified the mutational landscape progression in a patient's primary and recurrent GBM, and we uncovered Cas9-targetable repeat elements. We show that CRISPR-mediated targeting of highly repetitive loci enables rapid elimination of GBM cells, an approach we term "genome shredding." Importantly, in the patient's recurrent GBM, we identified unique repeat sequences with TMZ mutational signature and demonstrated that their CRISPR targeting enables cancer-specific cell ablation. "Cancer shredding" leverages the non-coding genome and therapy-induced mutational signatures for targeted GBM cell depletion and provides an innovative paradigm to develop treatments for hypermutated glioma.

Graphical Abstract

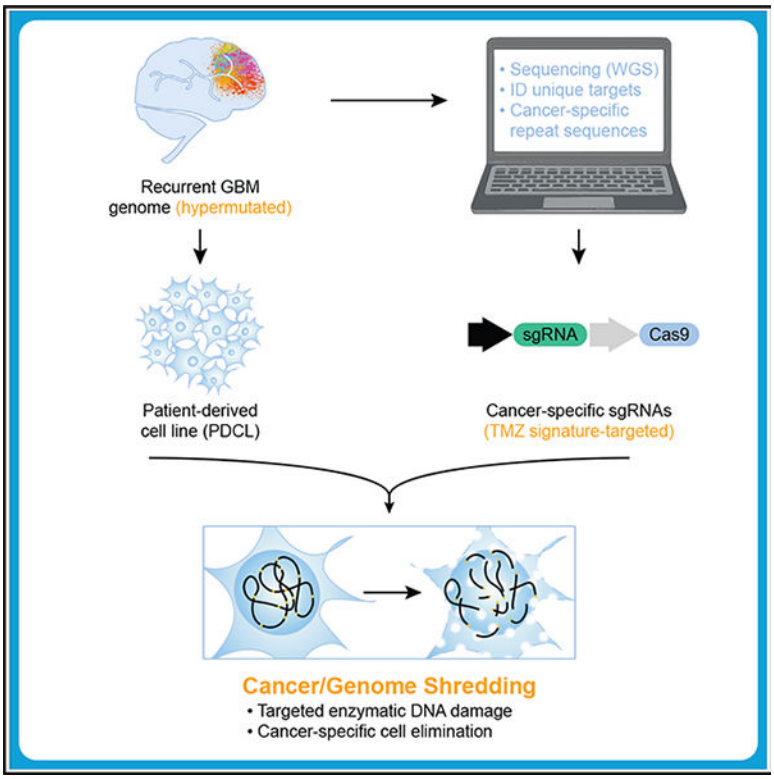

In brief

Tan et al. introduce "cancer shredding," a proof-of-concept CRISPR approach for treating recurrent glioblastoma. Utilizing personalized sgRNAs targeting repetitive non-coding sequences, including temozolomide chemotherapy-induced mutational signatures, they show rapid glioblastoma cell depletion. This offers a potential avenue to develop cancer-specific treatments for hypermutated gliomas and other hypermutated cancers.

INTRODUCTION

Primary glioblastoma (GBM) is a highly aggressive tumor of the central nervous system (CNS) that remains challenging to treat. Despite multimodal treatment regimens, median survival is 12–15 months.[1,2] GBMs are highly diffuse and infiltrate normal brain parenchyma, rendering complete surgical resection improbable. Growth of residual tumor inevitably occurs, mostly near the resection cavity and with therapy resistance.[3] Bulk and single-cell sequencing revealed that GBMs exhibit extensive intratumoral heterogeneity, with subpopulations of cells displaying distinct mutations, copy number aberrations, gene expression patterns, and epigenetic states.[4–6] This heterogeneity renders therapies targeted at specific molecular processes ineffective as it enables tumor recurrence from clones with distinct genetic makeups.[7]

Methylation status of the O-6-methylguanine-DNA methyltransferase (*MGMT*) promoter determines sensitivity to the alkylating agent temozolomide (TMZ), the current frontline chemotherapy for GBM.[2,8,9] While TMZ-based therapies show relatively few side effects and extend survival, most patients experience disease progression. At recurrence, 23% of *MGMT*-silenced GBM patients present with hypermutated tumors that correlate with dismal survival.[10] This percentage is higher for patients with recurrent astrocytomas and oligodendrogliomas. TMZ increases the rate of somatic mutation; coupled with tumor genomic instability and loss of DNA mismatch repair (MMR) pathways, this results in hypermutation.[10,11] Critically, no effective therapies currently exist against hypermutated gliomas. Hence, there is an urgent need for treatment strategies that can effectively eliminate GBM cells irrespective of their mutational and epigenetic profile.

Clustered regularly interspaced short palindromic repeats (CRISPR)-CRISPR-associated (Cas) methods, derived from bacterial and archaeal adaptive immune systems, enable RNA-guided introduction of DNA double-strand breaks (DSBs) at target loci throughout the genome.[12–16] Paired with reference and personalized genome information, CRISPR technologies enable programmable genetic manipulations in human cells.[17] One potential caveat of CRISPR therapies are cytotoxic effects due to the generation of DNA DSBs.[18,19] Large-scale genomic screens have shown that single-guide RNAs (sgRNAs) targeting amplified regions deplete more rapidly than controls. This effect is independent of sgRNA target site identities but dependent on the number of target sites present in a genome.[20–22] Interestingly, organ transplant-related efforts to inactivate porcine endogenous retroviruses resulted in up to 62 edits in an immortalized pig cell line and 25 edits in primary porcine cells that yielded living pigs.[23,24] Hence, it remains unknown how many DNA DSBs are required to efficiently eliminate a cell and whether such properties could be leveraged to use CRISPR as a potent anti-cancer modality.

Focusing on CNS cancer, here we propose that cytotoxic effects of DNA DSBs can be harnessed as a therapeutic strategy against recurrent hypermutated gliomas by targeting unique repeat sequences in tumor genomes, a concept we call CRISPR “cancer shredding.” We investigate the repeat threshold required for abolishing cancer cells using Cas9 targeted against non-coding elements. Additionally, we uncover that TMZ-induced hypermutation in recurrent GBM can lead to unique, cancer-specific repeat sequences. Importantly,

CRISPR targeting of these sequences led to selective depletion of a patient-derived recurrent GBM line, while sparing normal cells. Cancer shredding presents an innovative treatment paradigm independent of a tumor's genetic and epigenetic origin that converts the tumor mutational burden (TMB) and TMZ signature of hypermutated cancers into a possible avenue for treatment.

RESULTS

CRISPR leveraging of the non-coding genome

To comprehensively assess mutational landscape progression in an individual GBM, we compared a patient's primary and recurrent GBMs to their native genome using whole-genome sequencing (WGS) (Figure 1A). Upon initial diagnosis, the patient had undergone surgical resection as well as adjuvant radiotherapy and chemotherapy with TMZ. 11 months later, the patient relapsed. TMB quantification revealed a median of 123 mutations per megabase (Mb) for the primary tumor and 217 mutations per Mb for the recurrent GBM ($p < 0.01$, Wilcoxon rank sum, Figures S1A and S1B), categorizing both tumors as hypermutated.[10,25] By computational variants analysis using Mutect2,[26] we further identified 4,434 and 11,601 protein-coding mutations in the primary and recurrent GBM, respectively (Figure 1B). Notably, we found a far larger number of mutations (451,484 and 698,557, respectively) in the non-coding genome. As coding regions represent 1%–2% of the human genome,[27–29] this implies a similar mutational burden across the entire genome. Despite the considerable sequence space of the non-coding genome, current targeted therapies focus almost exclusively on protein-coding elements and their regulation. In GBM, this often results in recurrent tumors being unresponsive to initial treatments due to genetic differences from the primary tumor.[7] Hence, to track the patient's genomic tumor progression, we intersected all variants with the ClinVar database (NCBI) to identify variants at loci annotated as pathogenic or likely pathogenic (Table S1).

Closer inspection revealed two germline missense mutations in the genes *CHEK2* and *ARID1B* (Figure 1C). Both genes are involved in DNA damage response (DDR). *CHEK2* is a checkpoint kinase that acts as a tumor suppressor gene, and its mutation is implicated in various cancers, including gliomas.[30–33] *CHEK2* is associated with mismatch repair (MMR) through interaction with *MSH2*.[34] *ARID1B*, another tumor suppressor, is part of the SWI/SNF chromatin remodeling complex, and its alterations are linked to cancer, including neuroblastoma and gliomas.[35–37] Furthermore, both the primary and recurrent tumor had a somatic mutation in the *TERT*-promoter, referred to as "G228A." *TERT*-promoter mutations are the most common non-coding mutation in cancer, occur in ~83% of GBM, and enable binding of a GABPB1L-containing transcription factor complex that activates *TERT* expression.[38–43] Lastly, the recurrent tumor acquired a set of additional pathogenic mutations, including a known coding variant in the oncogene *PIK3CA*, a missense mutation in the methyltransferase *KMT2D* that is mutated in ~10% of cancer,[44] and a missense mutation in the MMR gene *MSH6*, a key driver of hypermutation in glioma.[10]

Overall, we uncovered germline deficiencies in DDR genes, which likely enabled the high mutational burden in the primary tumor, and a somatic mutation in the *TERT*-promoter critical for GBM cell immortalization. Moreover, the recurrent tumor is genetically divergent

from the primary GBM, with additional mutations linked to aggressive cancer progression and hypermutation. To explore alternative therapeutic strategies, we leveraged CRISPR and computed all possible *Streptococcus pyogenes* Cas9 (SpyCas9, 5′-NGG-3′ PAM) sgRNAs in the patient's native genome as well as primary and recurrent GBM (Figure 1D). Among the hundreds of millions of possible sgRNAs in this target space, termed "sgRNA-ome," we found a large proportion that had multiple target loci in the genome, with the highest ones targeting over 100,000 sites each.

We hypothesized that use of such sgRNAs could serve as a robust method for glioma cell depletion irrespective of the underlying mutational landscape. When computing the SpyCas9 repeat sgRNA-ome of the human reference genome (*Homo sapiens*, hg38), we observed a similar distribution of repetitive loci as in the patient's GBM genomes (Figure 1E). We refer to sgRNAs with highly repetitive target sites as "sgCIDEs," for CRISPR-induced death by editing.[45]

To better understand the origin of repetitive CRISPR loci, we annotated highly repetitive target sequences (>1,000 repeats). When aligned to annotation tracks of coding and non-coding elements (GENCODE v38, UCSC RepeatMasker), repeat sequences mostly mapped to the non-coding genome (Figures 1F and S1C). Functionally, they were often derived from retrotransposons and other transposable elements (TEs), constituting up to ~45% of the human genome, or microsatellites, accounting for ~3% of the human genome.[29,46] The TE class, representing the majority of repeat targets, was partitioned into two subgroups with differential representation among coding and non-coding genome (see inset, Figure 1F). In contrast, the microsatellite class did not show this separation. TE-based targets had either a primary association with long interspersed nuclear elements (LINEs; ~1%–3% in coding genome) or short interspersed nuclear elements (SINEs; <1% in coding genome).

We further assessed whether repetitive targets cluster in distinct genomic regions, but we observed a nearly uniform distribution throughout the genome, except for pericentromeric heterochromatin and stalks in acrocentric chromosomes (Figures 1G and S1D), which are often not fully represented in the human reference genome.[47] Hence, while highly repetitive sgRNA targets are spread throughout the genome, they are mostly associated with discrete repeat elements of TE origin in the non-coding genome.

Genome shredding enables rapid cell elimination

To investigate the ability of CRISPR-Cas9 to eliminate GBM cells through targeting of repetitive sequences, a strategy we term "genome shredding" (Figures 1A and 2A), we selected 10 of the most repetitive sgRNAs in the human genome (Figure 2B). For each sequence, featuring ~3,000–300,000 target sites per haploid genome, we further determined the number of off-target sites at Hamming distance (HD) of up to three and allowing for NGG or NAG PAMs (Table S2). Importantly, when tested in U-251 and LN-229 GBM cells, stable expression of Cas9 and all of the ten sgCIDEs led to rapid and robust cell depletion in competitive proliferation assays (Figure 2C). While cells expressing non-targeting sgRNAs (sgNT) did not deplete, sgCIDE-expressing cells depleted more rapidly than cells expressing sgRNAs targeting a consensus essential gene,[48] replication protein A1 (*RPA1*). To assess genome shredding in a more therapeutically relevant model, without pre-engineered Cas9

expression, we repeated these experiments in native U-251 and normal human astrocytes (NHAs) using an all-in-one Cas9-sgRNA vector (pCF827), and we observed comparable results (Figure S2A).

To interrogate genomic consequences of genome shredding, we conducted comet assays and ran DNA from lysed target cells on agarose-coated slides (Figure 2D). Single-cell analysis of Cas9-expressing U-251 and LN-229 revealed extensive genomic fragmentation (long tails) at 24 h post transduction with sgCIDE-1/2/3, while minimal degradation occurred for sgNT-1/2/3 controls (Figures 2E and 2F). Next, to assess dynamic effects of repetitive loci targeting, we used real-time quantitative live-cell imaging to monitor Cas9-expressing U-251 transduced with lentivirus expressing mNeonGreen-coupled sgCIDEs (sgCIDE-1/2/3/6/8/10) or sgNT-1/2/3 over 5 days (Figures 2G and S2B). Propidium iodide (PI) staining and live-cell quantification revealed that sgCIDEs induced growth inhibition starting at day 1 post transduction and cell death starting as early as day 2. Together, these experiments show that targeting of highly repetitive sequences is a reliable strategy for rapid elimination of GBM cells.

Genome shredding is agnostic to genetic and epigenetic origin

Active *MGMT* removes TMZ-added methyl groups from the O^6 position of guanines, rendering chemotherapy ineffective.[8,49] In GBM cells with promoter-methylated (silenced) *MGMT*, TMZ induces DNA damage and G2/M cell-cycle arrest, followed by p53-dependent cell death.[50] Hence, we investigated whether genome shredding is equally active in both TMZ-sensitive and -resistant GBMs. We treated Cas9-expressing TMZ-sensitive U-251 and LN-229 and TMZ-resistant T98G and LN-18 GBM cells with TMZ or transduced them with lentiviral vectors expressing sgCIDEs (Figures 3A and S3A). Quantification of cell viability over 5 days showed expected effects for TMZ dose titrations, with lethality observed only in U-251 and LN-229. In contrast, sgCIDE-1/2/3/6/8/10 expression induced viral titer-dependent lethality in all four GBM lines independent of *MGMT* promoter methylation status, while negative controls (sgNT-1/2) showed no effect.

To assess effects on cell-cycle progression, we treated cells with TMZ or sgCIDEs for 1–5 days and stained them with PI post fixation, followed by flow cytometry analysis (Figure 3B). Control DMSO and sgNT-1/2 treatments, as well as guide RNAs targeting a non-essential gene (olfactory receptor, sgOR2B6-1/2), showed comparable normal cell-cycle profiles in Cas9-expressing U-251, LN-229, T98G, and LN-18 (Figures 3C, 3D, and S3B). As expected, TMZ treatment (50 μM) showed the characteristic G2/M cell-cycle arrest and slow increase of the Sub-G1 population starting at day 2, but only in the TMZ-sensitive lines. Increase of the Sub-G1 population was more prominent in U-251 (RRID:CVCL_0021) carrying the common TP53 R273H mutation compared to LN-229 (RRID:CVCL_0393, TP53 P98L) that retain a functional *TP53* (Figure S3B). This reflects previous observations that *TP53* status affects resolution of the G2/M arrest.[50,51] Additionally, treatment with sgRNAs targeting the essential gene *RPA1* (sgRPA1-2/3) resulted in an accumulation in S-phase starting at day 3, accompanied by increase of the Sub-G1 population, in all four GBM lines.

In contrast, genome shredding with sgCIDE-1/2/3/6/8/10 led to a rapid increase of the Sub-G1 population starting at day 1 post transduction, combined with a drastic depletion of the G1 peak and slight increase of the S-phase population, in all four tested GBM lines (Figures 3C, 3D, and S3B). Notably, this change in cell-cycle profile was consistent across all six sgCIDEs and for all four GBM cell lines, independent of *MGMT* promoter methylation status and TMZ sensitivity. At day 2 post transduction, the Sub-G1 population of sgCIDE transduced samples already represented ~20%–40%, and ~30%–60% at day 3, a signal of rapid cell death.

To further evaluate genome shredding in systems that better model the therapy resistance seen in patients, we transduced glioblastoma stem-like cell (GSC) lines (GBM12, GBM85, GBM123) with all-in-one vectors (pCF827) expressing Cas9 and sgRNAs (sgNT-1/2/3, sgCIDE-1/2/3), and we assessed cell viability (Figure 3E). While TMZ (50 μM) treatment efficiency varied across the three GSC lines, sgCIDE-1/2/3 led to effective cell depletion in all cases. Thus, CRISPR-Cas genome shredding robustly induced cell death independent of the glioma cells' genetic and epigenetic makeup, suggesting versatility in dealing with intratumoral heterogeneity.

Genome shredding escape is non-trivial and can be rescued with repeat treatment

Recurrent tumors often develop from cells escaping treatment by avoiding therapeutic exposure or developing therapy resistance. To evaluate the robustness of genome shredding, we performed treatment regimens in colony formation assays (Figure 4A). Cas9-expressing U-251, LN-229, T98G, and LN-18 GBM cells were stably transduced with lentiviral vectors expressing sgNT-1/2 or sgCIDE-1/2 and seeded at low density in six-well plates. Controls were treated with DMSO or TMZ (50 μM). Crystal violet staining 2 weeks later revealed that TMZ treatment reduced colony numbers by about 1–2 log-scales compared to DMSO for U-251, while T98G grew unaffected (Figure 4B). As expected, treatment with sgNT-1/2 had little effect on colony formation. Conversely, genome shredding with sgCIDE-1/2 led to a 2–3 log-scales reduction in colony numbers across both GBM lines. Nevertheless, a few cells survived and formed colonies.

To better understand what happened with these "escapee" cells, and whether there are biological barriers to cell ablation by genome shredding, we designed a recurrent treatment assay (Figure 4A). We established monoclonal cell lines by isolating escapee clones (sgCIDE-1/2), as well as negative controls (sgNT-1), and expanded them under puromycin selection to ensure continued presence of the genomically integrated Cas9 constructs (EFS-Cas9-P2A-Puro). We further confirmed that all cell lines remained mNeonGreen positive, a marker for the sgRNA vector (U6-sgRNA EF1a-mNeonGreen). Overall, we prepared four clones each from U-251 and LN-229 escapees, as well as respective controls. To model recurrent treatment, we developed lentiviral vectors expressing an sgRNA and mCherry (pCF820) or an all-in-one version encoding an sgRNA and mCherry-tagged Cas9 (pCF826). For high-titer production of all-in-one vectors, we established a "CRISPR-safe" packaging cell line through stable overexpression of the anti-CRISPR protein AcrIIA4 (Figures S4A and S4B), using a lentiviral construct we previously built.[52]

Competitive proliferation assays showed that retreatment of escapee clones with vectors providing only a new sgRNA (pCF820; sgNT-1, sgCIDE-1/2) did not result in cell depletion (Figures S4C and S4D). However, retreatment with all-in-one vectors providing both a new sgRNA and Cas9 (pCF826) resulted in efficient cell ablation in all cases (Figures 4C and S4E). Interestingly, most (7/8) escapee clones could be retreated even with the Cas9-sgNT-1 control construct. Since all escapee clones were monitored for continued Cas9 expression (puromycin selection) and sgRNA vector presence (mNeonGreen+), this demonstrates that lack of a functional Cas9 was the key issue, with one escapee clone (U-251 sgCIDE-1 #1) also lacking a functional sgRNA, rather than a potential biological escape mechanism. We hypothesize that Cas9 was inactivated by in-frame mutation, similar to previous observations,[53] though further investigation is needed to confirm this. Such mutations could have arisen already during plasmid propagation or viral preparation, rather than after cellular integration.

To further investigate the potential of genome shredding in an *in vivo* tumor environment, we locally injected sgNT-1- or sgCIDE-1-expressing lentivirus (5 μL, 15 μL) into mice bearing Cas9-expressing LN-229 intracranial xenografts (Figure 5A). Prior to injection, we evaluated the efficacy of the concentrated virus *in vitro*, using Cas9-expressing LN-229, and we observed efficient cell transduction and destruction for sgCIDE-1 (Figure 5B). Postmortem flow cytometry analysis of tumors treated *in vivo* with sgNT-1 constructs revealed ~15%–20% mNeon-Green+ cells (5 μL: 8.9%–81.5%, 15 μL: 2.7%–32.1%). In contrast, tumors injected with sgCIDE-1 showed only ~0.2%–0.5% mNeonGreen+ cells (5 μL: 0.0%–0.4%, 15 μL: 0.0%–0.9%), indicating that the vast majority of *in vivo* sgCIDE-1 transduced cells were effectively eliminated (Figure 5C). However, Kaplan-Meier analysis revealed no survival benefit of sgCIDE-1-treated groups (Figure 5D), suggesting that the therapeutic delivery was insufficient and that elimination of ~15%–20% of tumor cells does not prolong overall survival.

To bypass delivery limitations and potentially achieve a more pronounced effect, we developed a tamoxifen-inducible Cas9 system, termed “TiCas9,” based on arC9 variants.[54] After evaluating TiCas9’s 4-hydroxytamoxifen-induced (4-OHT, 3 days) editing potential in GFP-containing HEK293T cells (Figure 5E), we assessed genome shredding efficiency with sgCIDE-1/2/3 in TiCas9-encoding U-251 (Figure 5F). While we did not observe any leakiness under DMSO conditions, 4-OHT treatment led to strong TiCas9 editing activity, albeit not fully matching wild-type Cas9 levels. Next, we established intracranial xenografts from TiCas9 and sgNT-1/sgCIDE-1 encoding U-251 and treated them with tamoxifen (100 mg/kg per day for 5 days), starting 1 week after tumor implantation (Figure 5G). Overall, Kaplan-Meier analysis, with cohorts of four and five mice, revealed a slight survival benefit of the sgCIDE-1-treated group, though not quite significant ($p = 0.0528$). Together, these results demonstrate genome shredding-based tumor cell ablation in an *in vivo* microenvironment and support its potential as a therapeutic approach for brain cancer treatment. However, further optimization of delivery methods and combination with complementary strategies will be necessary to enhance its impact on overall survival.

Minimal determinants of effective cell ablation

To delineate parameters of genome shredding, we set out to probe the minimum number of target repeats needed to effectively eliminate a cell. Generally, each target locus will lead to a CRISPR-induced DSB, followed by cellular repair through non-homologous end-joining or homology-dependent repair or, if there is substantial DNA damage, cell death. However, target loci lead to DNA DSBs with varying efficiency depending on the sequence of the sgRNA,[55] the complementarity of the sgRNA to the target sequence,[56,57] and—to a lesser degree—the chromatin accessibility of the target site.[58,59] Thus, to assess cell depletion efficiencies of sgCIDEs in eukaryotic cells with varying amounts of endogenous target sites, we tested a set of sgRNAs in human, mouse, and chicken genomic backgrounds (Figure 6A).

In addition to the human sgRNAs, we computed all SpyCas9 (5′-NGG-3′ PAM) sgRNAs for mouse (*Mus musculus*, mm10) and chicken (*Gallus gallus*, galGal6) genomes and enumerated sgRNA occurrences (Figure S5A). Next, we quantified the number of target sites with full complementarity (HD 0) or one to three mismatches (HD 1–3) across all three genomes and selected a set of sgRNAs for a DSB-induced cell death assay (Figures 6B and S5B, Table S2). Beyond non-targeting control sgRNAs (sgNT-1/2/3), we chose three top human sgRNAs with fewer targets in the mouse genome and no targets in the chicken genome (sgCIDE-1/2/3), four sgRNAs that target only the mouse genome (sgCIDE-21/22/23/24), six sgRNAs targeting the human and mouse genome (sgCIDE-31/32/33/34/35/36), and six microsatellite-targeting (k-mer repeat) sgRNAs (sgCIDE-41/42/43/44/45/46) with high target counts in all three genomes.

Competitive proliferation assays in Cas9-expressing human U-251 GBM, mouse GL261 GBM, and chicken DF-1 fibroblast cells demonstrated that pan-vertebrate sgCIDEs (#41-46) rapidly deplete transduced cells independent of the species (Figures 6C, S5C, and S5D). Beyond the minimal number of 32 fully matching (HD 0) target sites in this set (sgCIDE-44, chicken genome), we noted little correlation between cell death and the number of target sites, though all sgRNAs had at least several hundred target sites when counting loci with single mismatches (HD 1). Additionally, the top human sgRNAs (sgCIDE-1/2/3) also efficiently eliminated mouse GBM cells despite having only ~70–100 target sites with a single mismatch (HD 1) and only two fully complementary sites. Similarly, sgRNAs with hundreds of target sites in the human genome (HD 0) were equally efficient at depleting target cells as sgRNAs with hundreds of thousands of target sites. While it remains difficult to accurately determine the number of DSBs needed for efficient cell elimination, these results suggest that a minimum of ~30 fully complementary target sites or ~70 target sites with a single mismatch is sufficient.

Leveraging mutational signatures in hypermutated GBM for targeted oncolysis

Since the targets used above for genome shredding are also present in normal genomes, regional specificity would have to be provided by localized delivery, as is the case with radiotherapy and surgery.[3] However, we hypothesized that cancer-specific mutations in hypermutated gliomas might lead to unique sequences that can be exploited for cancer-specific genome fragmentation, a process we termed “cancer shredding” (Figure 7A). Concretely, following rounds of TMZ treatment, GBMs often relapse as hypermutated

tumors with characteristic cytosine-to-thymine (C>T) conversions mainly due to a combination of TMZ exposure and acquired MMR pathway deficiency.[10,11] These mutations render the genomic landscape of recurrent gliomas distinct from the patient's native genome and should enable exclusive CRISPR targeting.

To assess whether such mutations exist, we analyzed the patient's primary and recurrent GBM, as well as native genome. Quantification of the mutational landscape across the coding and non-coding genome revealed stereotyped signatures not only in the primary and recurrent GBM but also in the native genome (Figure S6A). Both the native genome and primary GBM showed a high prevalence of C>T and T>C mutations, a signature associated with germline MMR deficiency in absence of distinct exogenous stressors.[60] Additionally, the recurrent GBM showed a specific increase in C>T conversions, consistent with TMZ chemotherapeutic stress.[10] When accounting for the mutational background present in the patient's native genome, the recurrent GBM displayed the characteristic TMZ mutational signature (signature 11)[11,61] of hypermutated GBM (Figure 7B).

To determine whether TMZ signature mutations can be leveraged for GBM-specific targeting and cell ablation, we utilized a cell line derived from the patient's recurrent GBM (Figure 7A), established by the UCSF Brain Tumor Center Preclinical Therapeutics Core. Next, we assessed the sensitivity of this hypermutated patient-derived cell line (PDCL, SF11411) to general genome shredding and observed effects similar to other GBM lines (Figure S6B). To ensure that the SF11411 line represents the patient's recurrent tumor, and not a distant sub-clone, we ran WGS and computed a list of recurrent GBM-specific sgRNAs ("sgRECs"). The mutational landscape of the SF11411 PDCL correlated well with that of the patient's recurrent GBM tissue (Figure 7C). For inclusion in the recurrent GBM sgRNA-ome, an sgRNA target sequence had to be found in both PDCL sequencing replicates and have a single mismatch at positions 1–8 from the PAM compared to the patient's native genome. Specifically, the candidate sgRNAs had zero targets at HD 0 and only one target at HD 1 in both the patient's native and reference (hg38) genomes. Importantly, we also identified cancer-specific repeat sgRNAs by computing targets that were both repetitive in the recurrent cancer and unique to the recurrent cancer (mismatch at positions 1–8 from PAM); we uncovered 10 sgRNAs that meet these criteria (Figure 7D, Table S3).

To validate our cancer-specific sgRNA predictions, we carried out a large-scale CRISPR screen in NHAs versus the SF11411 PDCL (Figure 7A). Our library included guides targeting the coding and non-coding genome at a single site or multiple loci (including cancer repeat sgRNAs), all sgCIDEs, ~80 non-targeting controls, and ~1,000 safe-harbor references (with no off-targets up to HD 3) for a total of ~5,000 sgRNAs (Table S3). We compared NHAs and SF11411s transduced at single copy (35% for NHA, 11% for SF11411) with the CRISPR library by next-generation sequencing at day 1 (T0) and 28 days (D28) post transduction (14 cell doublings). As expected, most sgCIDEs were strongly depleted in both cell lines, with the exception of the mouse-specific sgCIDE-21/22/23/24 and some sgCIDE-2/3 replicates that showed amplification biases in NHAs (Figures 7E and S6C). More importantly, while the non-targeting controls behaved neutrally in both lines, the

cancer repeat sgRNAs strongly depleted only in the SF11411 line while ending up enriched in NHAs.

To further quantify cancer-specific sgRNA depletion, we used the MAGeCK pipeline for statistical analysis.[62] Among all sgRNAs in the CRISPR screen, the cancer repeat sgRNAs were most strongly depleted specifically only in the hypermutated SF11411 GBM cells (Figure 7F, Table S3). Using gene-level statistics and FDR <0.05, the cancer repeat sgRNAs consistently emerged as the most depleted set (Figure 7G). This highlights that TMZ signature mutations in hypermutated recurrent glioma can result in unique repeat sequences that enable selective CRISPR targeting of tumor cells and effective cancer shredding.

While this patient presented with a rare germline DDR deficiency and high mutational burden already in the native genome, we believe that for patients with acquired MMR deficiency and a lower baseline burden of C>T mutations (Figure S6A), it should be possible to identify more hypermutated glioma-specific repeat sgRNAs (personalized cancer-specific repeat sgRNAs). This should hold particularly true for hypermutated astrocytomas and oligodendrogliomas that accumulate mutations over an extended period of time.[63] Taken together, cancer shredding provides a promising therapeutic concept for difficult-to-treat glioma and possibly other hypermutated tumors.

DISCUSSION

Therapies for gliomas have made muted progress over the past decades,[3] with alternative strategies being critically needed. Here we introduce CRISPR-mediated genome and cancer shredding as a conceptual paradigm to treat recurrent gliomas. Cancer shredding leverages CRISPR as anti-cancer modality through targeting of repetitive tumor-specific loci, leading to genome fragmentation and DNA damage-induced cell death. Specifically, we found that ablation of GBM cells by genome shredding is rapid and efficient. We further showed that genome shredding works independent of a GBM cell's epigenetic status and sensitivity to frontline TMZ chemotherapy. Additionally, while most targeted cells succumb to initial DNA damage introduced by genome shredding, we demonstrated that rare escapee clones can effectively be retreated, suggesting the possibility for multi-cycle regimens.

Compared to conventional approaches, CRISPR strategies enable the vast space of the non-coding genome and non-driver mutations to serve as targets. While protein-coding sequences occupy 1%–2% of the human genome, with driver genes being a small fraction of that,[64] repeat elements make up over 50%.[29] Accordingly, our data illustrate that the majority of the genomic sequence and variant space can serve as potential guide RNA targets for genome shredding. Moreover, the existence of tumor-specific repeat sequences could enable targeted cancer shredding without the need for cell type-specific delivery. Analyzing the patient's cancer by WGS, we identified unique recurrent GBM-specific sgRNAs. The targets of these sgRNAs, mainly in the non-coding genome, were generated by TMZ signature mutations characteristic of hypermutated gliomas.[10,11] Importantly, using a large-scale CRISPR screen, we demonstrated that cancer shredding enables selective elimination of hypermutated recurrent patient-derived GBM cells through targeting of therapy-induced

TMZ signature mutations. This suggests an alternative avenue for therapeutic development that has heretofore not been explored.

Prior work has shown that collateral nuclease activity of Cas13 can be exploited to inhibit the growth of certain cancer cells.[65] However, since Cas13 targets RNA, this approach only permits targeting mutations in expressed regions of the genome and restricts the sequence space by excluding large sections of the non-coding and coding genome.

While the sgRNAs employed here for cancer shredding are personalized to this patient's recurrent GBM, we believe that identifying cancer-specific sgRNAs will be feasible for many patients with recurrent hypermutated gliomas, particularly those with acquired MMR deficiency. As hypermutated astrocytomas and oligodendrogliomas accumulate mutations over a prolonged period of time following MMR loss and TMZ treatment (years rather than months), they often have a higher TMB compared to hypermutated GBMs.[63] Additionally, the native genome of most patients (without germline DDR/MMR deficiencies) will contain fewer pre-existing C>T mutations (Figure S6), making the TMZ signature mutations more prominent. Together, this should facilitate the identification of effective cancer-specific repeat sgRNAs.

However, clinically viable CRISPR delivery modalities remain a challenge for many applications. This limitation was manifest with the poor overall efficacy of glioma lysis with direct sgRNA injections compared to induction of a CRISPR-transgenic xenograft in our mouse models (Figures 5D and 5G). The results' disparity highlights the current difficulty of effective *in vivo* CRISPR delivery and reinforces the need for further developments in this area in order to enable safe and effective clinical implementation of cancer shredding. Notably, recent work has shown promising editing efficiencies in the brain by delivery of prime editing systems using dual AAVs.[66] Additionally, convection-enhanced delivery combined with various CRISPR encapsulation strategies might provide a parallel avenue to increase delivery efficiency.[3]

Despite the current lack of effective delivery modalities, cancer shredding establishes an innovative conceptual approach to tackle late-stage hypermutated gliomas through leveraging the non-coding genome and TMZ signature mutations. Beyond salvage therapy for recurrent gliomas, cancer shredding could enable non-systemic neo-adjuvant treatment paradigms to shrink hypermutated tumors prior to surgical resection. The general challenge of delivery notwithstanding, local stereotactic administration could facilitate treatment of tumors that are either too small to resect or are situated in regions of the brain where surgical resection is undesirable (Figure 7H). Of note, the injury and destruction of tumor genomes by cancer shredding might boost immunotherapy in combating disease progression. Ultimately, CRISPR-mediated cancer shredding provides an innovative therapeutic concept for patients with hypermutated gliomas and possibly other cancers with hypermutated genomes.

Limitations of the study

In this work, we demonstrate that Cas9 targeting of highly repetitive elements in the non-coding genome enables rapid cell elimination. Quantifying a patient's primary and recurrent

GBM, we further show that hypermutated gliomas can contain unique repeat sequences with TMZ signature mutations. We provide proof of concept that CRISPR-mediated targeting of these sequences enables cancer-specific cell ablation, a strategy we termed “cancer shredding.” For safe and effective clinical implementation of this approach, delivery remains a major challenge. This study does not address delivery limitations nor establish a path for direct clinical implementation of the presented concept.

STAR★METHODS

Detailed methods are provided in the online version of this paper and include the following:

RESOURCE AVAILABILITY

Lead contact—Further information and requests for resources and reagents should be directed to and will be fulfilled by the lead contact, Christof Fellmann (christof.fellmann@gladstone.ucsf.edu).

Materials availability—Reagents used in this study are publicly available (Addgene), from commercial sources, or available from the lead contact upon reasonable request.

Data and code availability

- CRISPR screen data have been deposited to the Gene Expression Omnibus (https://www.ncbi.nlm.nih.gov/geo/) under the accession code GSE244497.
- Code written specifically for this project can be found at the following repository: https://bitbucket.org/arp2012/cell_reports_2023/src/master/
- Any additional information required to reanalyze the data reported in this paper is available from the lead contact upon request.

EXPERIMENTAL MODEL AND STUDY PARTICIPANT DETAILS

Mammalian cell culture—All mammalian cell cultures were maintained in a 37°C incubator at 5% CO_2. HEK293T human kidney cells (293FT; Thermo Fisher Scientific, #R70007; RRID:CVCL_6911), HEK-RT1 (a monoclonal HEK293T cell line expressing a doxycycline-inducible GFP),[45] DF-1 chicken fibroblast cells (ATCC, #CRL-12203; RRID:CVCL_0570), normal human astrocytes (NHAs; culture option 1, used for cell line establishment), and derivatives thereof were grown in Dulbecco’s Modified Eagle Medium (DMEM; Corning Cellgro, #10-013-CV) supplemented with 10% fetal bovine serum (FBS; Seradigm #1500-500), and 100 Units/ml penicillin and 100 μg/mL streptomycin (100-Pen-Strep; Gibco, #15140-122). U-251 human glioblastoma cells (Sigma-Aldrich, #09063001; RRID:CVCL_0021), LN-229 human glioblastoma cells (ATCC, #CRL-2611; RRID:CVCL_0393), T98G human glioblastoma cells (ATCC, #CRL-1690; RRID:CVCL_0556), LN-18 human glioblastoma cells (ATCC, #CRL-2610; RRID:CVCL_0392), SF11411 hypermutated recurrent glioblastoma patient-derived cell line (PDCL) cells, GL261 mouse glioblastoma cells, normal human astrocytes (NHAs; culture option 2, used for experiments and CRISPR screen), and derivatives thereof were cultured in Dulbecco’s Modified Eagle Medium/Nutrient Mixture F-12 (DMEM/F-12;

Gibco, #11320-033) or Dulbecco's Modified Eagle Medium and Ham's F-12 (DMEM/F-12; Corning Cellgro, #10-090-CV) supplemented with 10% FBS and 100-Pen-Strep. Glioblastoma stem-like cell lines (GSCs) GBM12, GBM85, and GBM123, were obtained from the Mayo Clinic Brain Tumor PDX national resource. GSCs were cultured in Neurocult NS-A Basal Medium (Stemcell Technologies; #05751), B27 Supplement minus vitamin A (ThermoFisher; #12587010), N2 Supplement (ThermoFisher; #17502001), GlutaMAX (ThermoFisher; #35050061), Sodium Pyruvate (ThermoFisher; #11360070), and Penicillinstreptomycin (ThermoFisher; #15140122) supplemented with 20 ng/mL EGF (ThermoFisher; #PHG0311), and 20 ng/mL FGF (PeproTech; #100-18B). GSCs were grown in monolayers in laminin-coated plates. U-251, LN-229, T98G, LN-18, and HEK293T cells were authenticated using short tandem repeat DNA profiling (STR profiling; UC Berkeley Cell Culture/DNA Sequencing facility). STR profiling was carried out by PCR amplification of nine STR loci plus amelogenin (GenePrint 10 System; Promega, #B9510), fragment analysis (3730XL DNA Analyzer; Applied Biosystems), comprehensive data analysis (GeneMapper software; Applied Biosystems), and final verification using supplier databases including American Type Culture Collection (ATCC) and Deutsche Sammlung von Mikroorganismen und Zellkulturen (DSMZ). U-251, LN-229, T98G, LN-18, and HEK293T cells were tested for absence of mycoplasma contamination (UC Berkeley Cell Culture facility) by fluorescence microscopy of methanol fixed and Hoechst 33258 (Polysciences, #09460) stained samples.

The SF11411 PDCL was derived from the patient's recurrent hypermutated glioblastoma tissue (David Raleigh, Tomoko Ozawa, and Kyounghee Seo; UCSF Brain Tumor Center Preclinical Therapeutics Core). The UCSF Institutional Review Board approved the use of human material presented in this work. Written informed consent was obtained from the patient. The normal human astrocyte cell line NHA-N2, here simply referred to as "NHA", is puromycin sensitive and GFP/ZsGreen negative. The monoclonal NHA-N2 cell line was derived from NHA-PC5 cells that are puromycin resistant and ZsGreen positive,[67] through CRISPR deletion of the previously inserted puromycin and ZsGreen cassettes. The NHA-PC5 cells were edited by transduction with virus-like particles (VLPs)[69] containing Cas9 and sgPuro-5/6 or sgZsGreen-2/3 (Table S2).

Mice—Athymic nude mice (*Foxn1*$^{nu/nu}$; IMSR_JAX:007850) mice were purchased from the Jackson Laboratory. All experiments were conducted in 6–10-week-old female mice. All animal experiments were conducted in accordance with the guidelines and regulations of the Institutional Animal Care and Use Committees at the University of California San Francisco.

METHOD DETAILS

Expression vectors—The lentiviral vector pCF226, expressing *Streptococcus pyogenes* Cas9 and a puromycin selection marker, was described previously.[45] The lentiviral vector pCF823, expressing *Streptococcus pyogenes* Cas9 and a puromycin selection marker, was cloned based on the insert of pCF226 and the optimized lentiviral backbone of pCF821. Of note, the pCF823 (Cas9-Puro) vector yields higher viral titers than the otherwise comparable pCF226 (Cas9-Puro) vector. The lentiviral vector pCF821, encoding a U6-sgRNA cassette

and an EF1a driven mNeonGreen marker, was derived from the pCF525 backbone[52] and the pCF221-based U6-sgRNA-EF1a-mCherry insert.[45] The mCherry fluorescence marker was replaced with a human codon optimized version of mNeonGreen (gBlock, Integrated DNA Technologies). Analogously, the lentiviral vector pCF820, encoding a U6-sgRNA-EF1a-mCherry2 cassette, was derived from pCF821 by replacing the mNeonGreen marker with a human codon optimized version of mCherry2 (gBlock, Integrated DNA Technologies). Of note, both the pCF820 (mCherry2) and pCF821 (mNeonGreen) sgRNA vectors yield higher viral titers than the otherwise comparable sgRNA vector pCF221 (mCherry). The all-in-one lentiviral vector pCF822, featuring a U6-sgRNA and EFS-Cas9-Puro cassette, was derived from pCF820 with an EFS-Cas9-Puro insert from pCF226 [45]. The all-in-one lentiviral vector pCF826, featuring a U6-sgRNA and EFS-Cas9-mCherry2 cassette, was derived from pCF822 by replacing the puromycin selection marker with mCherry2 from pCF820. The all-in-one lentiviral vector pCF827, featuring a U6-sgRNA and EFS-Cas9-mNeonGreen cassette, was derived from pCF822 by replacing the puromycin selection marker with mNeonGreen from pCF821. Vector sequences are provided (Table S2).

Tamoxifen-inducible Cas9 (TiCas9)—We established a tamoxifen-inducible Cas9 system, referred to as “TiCas9”, for regulated *in vitro* and *in vivo* Cas9 expression. The lentiviral vector pCF287 encodes a modified CBX3 ubiquitous chromatin opening element (UCOE) from pCF806 [70] and an EFS-TiCas9-P2A-Puro cassette. TiCas9 is based on an allosterically regulated Cas9 (ArC9)[54] that contains an estrogen receptor ligand-binding domain (ER-LBD) inserted within the Cas9 CDS. To improve tamoxifen responsiveness and editing efficiency, ArC9 was modified by combining the ER-LBD mutations referred to as ER-T2 (G400V/M543A/L544A)[71] with the V376A mutation[72] assumed to change the interaction with ER helix 12, and optimizing codon usage. Vector sequences are provided (Table S2). For *in vitro* assays we used 4-OHT (1 μM in 0.1% DMSO; (Z)-4-Hydroxytamoxifen, Sigma-Aldrich #H7904) to induce TiCas9. We use Tamoxifen, a prodrug that is metabolically converted to its active form 4-OHT, for *in vivo* studies.

To evaluate TiCas9 editing potential, HEK-RT1 cells were transduced with WT Cas9 (pCF226) or TiCas9 (pCF287), selected on puromycin (1.0 μg/mL), and further transduced with the indicated sgRNAs (pCF221; sgNT-1/2, sgGFP-8/9). Cells were then treated with DMSO (0.1%) or 4-OHT (1 μM in 0.1% DMSO; (Z)-4-Hydroxytamoxifen, Sigma-Aldrich #H7904, changed every day) for three days, followed by 24 h of doxycycline treatment (1 μg/mL) to induce GFP expression. Editing efficiency was quantified by flow cytometry of GFP expression.

Design and cloning of sgRNAs—All sgRNAs were designed with a G preceding the 20-nucleotide spacer for better expression from U6 promoters. All sgRNA sequences were cloned into the pCF820, pCF821, pCF826, and pCF827 vectors using Esp3I restriction sites and enzymes (New England Biolabs).

Viral transduction and generation of Cas9-expressing cell lines—Generally, lentiviral particles were produced in HEK293T cells or derivatives thereof using polyethylenimine (PEI; Polysciences, #23966) mediated transfection of plasmids, as previously described.[45] In brief, lentiviral transfer vectors were co-transfected with the

lentiviral helper plasmid psPAX2 (a gift from Didier Trono; Addgene, #12260) and the VSV-G envelope plasmid pMD2.G (a gift from Didier Trono; Addgene, #12259). Transfection reactions were assembled in reduced serum media (Opti-MEM; Gibco, #31985-070). For lentiviral particle production on 6-well plates, 1 μg lentiviral vector, 0.5 μg psPAX2 and 0.25 μg pMD2.G were mixed in 0.4 mL Opti-MEM, followed by addition of 5.25 μg PEI. After 20–30 min incubation at room temperature, the transfection reactions were dispersed over the HEK293T cells. Media was changed 12–14 h post-transfection, and virus harvested at 42–48 h post-transfection. Viral supernatants were filtered using 0.45 μm polyethersulfone (PES) membrane filters, diluted in cell culture media as appropriate, and added to target cells. Polybrene (5 μg/mL; Sigma-Aldrich) was supplemented to enhance transduction efficiency, if necessary. Importantly, unless described otherwise, all-in-one vectors encoding Cas9-sgRNA (e.g., sgCIDE) combinations were produced using the here established CRISPR-Safe packaging cell line to enable high viral titers. Cell lines stably expressing *Streptococcus pyogenes* Cas9 were generated by transduction with the lentiviral vector pCF226 or pCF823, followed by selection on puromycin (1–2 μg/mL; Invivogen, #ant-pr-1). To generate LN229-Luc-mCherry-Cas9 cells for *in vivo* experiments, we employed a two-round transduction strategy. First, LN229 cells were transduced with luciferase-IRES-mCherry lentivirus (GeneCopoeia, #LPP-HLUC-Lv214-100-C). The mCherry+ cells were then isolated by flow cytometry and subsequently transduced with pCF823 to generate LN229-Luc-mCherry-Cas9 cells.

CRISPR-safe packaging cells—To prevent viral packaging cells from dying when transfecting all-in-one Cas9-sgRNA vectors expressing sgCIDEs, HEK293T human embryonic kidney cells (293FT; Thermo Fisher Scientific, #R70007; RRID:CVCL_6911) were transduced with the lentiviral vector pCF525-AcrIIA4[52,73] to stably express the anti-CRISPR protein AcrIIA4, a potent inhibitor of *Streptococcus pyogenes* Cas9.[74] Transduced cells were selected on Hygromycin B (400 μg/mL; Thermo Fisher Scientific, #10687010) and the resulting cell line termed “CRISPR-safe” packaging cells.

Competitive proliferation assay—To assay the effect of Genome Shredding on cell viability and depletion, U-251, LN-229, T98G, LN-18, SF11411, NHA, GL261, and DF-1 cells with or without Cas9 expression were transduced at ~50–70% efficiency with lentiviral vectors to deliver mNeonGreen tagged sgRNAs (sgNTs, sgRPA1s, sgCIDEs). The percentage of mNeonGreen+ cells was quantified by flow cytometry (Attune NxT flow cytometer, Thermo Fisher Scientific) at 1, 2, 3, 5, and 7 days post-transduction (or as indicated). To test the effect of Genome Shredding using an all-in-one vector, U-251 cells were transduced at ~30% efficiency with pCF827 lentiviral vector to deliver mNeonGreen tagged Cas9 and sgRNAs (sgNT-1/2/3, sgCIDE-1/2/3). The percentage of mNeonGreen+ cells was quantified by flow cytometry at 2, 4, and 6 days post transduction.

To assay the cell elimination efficacy of Genome Shredding using TiCas9, TiCas9-expressing U-251 cells were stably transduced at approximately 50–70% efficiency with lentiviral vectors carrying mNeonGreen-tagged sgRNAs (sgNT-1/2/3, sgCIDE-1/2/3). Cells were then treated with 4-OHT (1 μM, renewed every day). The percentage of mNeonGreen+

cells was quantified by flow cytometry before treatment (day –1) as well as at day 1, 3, and 5 post 4-OHT treatment.

Comet assay—To detect DNA double-strand breaks (DSBs), a neutral comet assay was conducted following the manufacturer's protocol of the Comet Assay kit (Trevigen; Cat# 4250-050-K). In short, Cas9-expressing U-251 and LN-229 cells were transduced with lentiviral vectors expressing sgNTs or sgCIDEs (with 5 μg/ml of polybrene). Cells were collected 24 h post-transduction at a concentration of 1×10^5/mL, embedded in molten LMAgarose at a ratio of 1:10 (v/v), and transferred onto a CometSlide. Slides were immersed in Lysis solution at 4°C overnight. The next day, slides were washed in 1X TBE buffer, and gel electrophoresis using TBE buffer was performed (22 V, 20 min). Slides were then fixed in 70% ethanol for 5 min, dried at 37°C for 15 min, and stained with SYBR safe for 30 min. Images were taken using fluorescence microscopy. Comet tail length (in pixels) of individual cells was quantified using ImageJ. Each comet tail length was measured from the bottom of the comet head.

Live cell imaging with Incucyte SX5 Live-Cell Analysis Instrument—Cas9-expressing U-251 and LN-229 were plated at low density in a 96 well plate a day before live cell imaging. Right before transferring the 96-well plate into an Incucyte SX5 Live-Cell Analysis Instrument, cells were transduced with lentiviral vectors to express mNeonGreen-tagged sgRNAs (sgNT-1/2/3 and sgCIDE-1/2/3/6/8/10). Propidium iodide (PI) staining solution (Invitrogen) was also added to each well to visualize dying cells. Images (20X) were taken every 30 min until day 5 post-transduction. The number of mNeonGreen+ cells at each timepoint was calculated by the Incucyte SX5 Live-Cell Analysis Instrument.

Cell viability assay—To determine the effect of different treatments on cell viability, 1,000–2,000 Cas9-expressing U-251, LN-229, T98G, and LN-18 cells were plated in a 96-well plate. After an overnight incubation, cells were treated with different concentrations of TMZ (12.5–400 μM) or different dilutions of lentiviral vectors expressing sgNTs or sgCIDEs (with 5 μg/mL of polybrene). Cell viability was assessed at 1, 3, and 5 days post-treatment using the CellTiter-Glo Luminescent Cell Viability Assay (Promega, #G7572). To determine the effect of Genome Shredding on the viability of GSCs (GBM12, GBM85, and GBM123), 2000–4000 cells were plated in 96-well laminin-coated plates. After an overnight incubation, cells were treated with DMSO, 50 μM TMZ, or all-in-one lentiviral vectors to deliver Cas9 and sgRNAs (sgNT-1/2/3, sgCIDE-1/2/3; with 5 μg/mL of polybrene). Cell viability was measured at 5 days post-treatment using the CellTiter-Glo assay. In brief, 20 μL of CellTiter-Glo reagent was added to the well containing cells in 100 μL of cell culture medium. The plates were incubated at room temperature for 25 min and the luminescent signal was measured using a multimode microplate reader. The assay was performed in triplicate for each experiment.

Cell cycle analysis—To conduct cell cycle analysis and measure DNA fragmentation (sub-G1), ~2×10^4 Cas9-expressing U-251, LN-229, T98G, and LN-18 cells were plated in 24 well plates. The next day, cells were treated with DMSO, TMZ (50 μM), or lentiviral vectors expressing mNeonGreen-tagged sgNTs, sgOR2B6s, sgRPA1s, or sgCIDEs (with 5

μg/mL of polybrene). Cells were collected at 1-, 2-, 3-, 5-day post-treatment for cell cycle analysis using FxCycle PI/RNase Staining Solution (Invitrogen, #F10797). In short, cells were fixed in cold 70% ethanol for at least 1 h at −20°C, washed twice with PBS, and resuspended in 500 μL of FxCycle PI/RNase Staining Solution. Samples were incubated for 15 min at room temperature before being analyzed by a flow cytometer.

Colony formation assay—To perform colony formation assays, 100, 1,000, and 10,000 Cas9-expressing U-251, LN-229, T98G, and LN-18 cells were plated in 6 well plates. Cells were treated with DMSO, TMZ (50 μM), or lentiviral vectors expressing sgNTs or sgCIDEs (with 5 μg/ml of polybrene) the next day. The cell culture medium was changed every 3–5 days. Two weeks after the treatment, cells were fixed in 4% PFA for 15 min at room temperature, washed with PBS twice, and stained with 0.005% crystal violet for 20 min. Cells were then washed with dH_2O three times before imaging.

Virus preparation for in vivo experiments—We generated pCF821-sgNT-1 and pCF821-sgCIDE-1 lentivirus using six 10 cm plates of HEK293T cells. Per 10 cm plate, 8 μg of lentiviral vector, 4 μg of psPAX2 and 2 μg of pMD2.G were mixed in 2 mL Opti-MEM. Then, 42 μg polyethyleneimine (PEI; Polysciences #23966) was added to the mixture and incubated at room temperature for 25 min. The transfection mixture was then added to the 10 cm plate. Media was changed 16–18 h after transfection, and virus was harvested 48 h post-transfection. Viral supernatants were collected and filtered through 0.45 μm PES membrane filters to remove debris. The filtered supernatants were pooled and centrifuged at 25,000 rpm, 4°C for 2 h using the SW28 rotor in an ultracentrifuge (Beckman). After centrifugation, the viral pellet was resuspended in 150 μL of D-PBS and transferred to a 1.5 mL tube. The viral suspension was then centrifuged at 10,000 rpm, 4°C for 2 min to remove any remaining debris. Finally, the virus was aliquoted into 25 μL/tube and stored at −80°C until use.

Orthotopic tumor xenografts—For the *in vivo* competitive proliferation experiments, we first established intracranial tumor xenografts by injecting 2 × 10^5 LN229-Luc-mCherry-Cas9 cells (in 2 μL; 1 μL/min) into the striatum of female athymic nude mice (*Foxn1*$^{nu/nu}$) at the following coordinate: AP +0.5 mm, ML +1.8 mm, DV −4mm relative to bregma, using a 27 gauge Hamilton syringe and automated stereotaxic equipment (NEUROSTAR Drill and Injection Robot). After one week, 5 μL or 15 μL of concentrated lentivirus (pCF821-sgNT-1 or pCF821-sgCIDE-1) was injected by continuous convection-enhanced delivery (CED) into the tumor, at the same coordinate, via a CED needle at a rate of 1 μL/min.

For the TiCas9 experiment, we established intracranial tumor xenografts by injecting 3 × 10^5 U-251-TiCas9-sgNT-1 or U-251-TiCas9-sgCIDE-1 cells (in 3 μL; 1 μL/min) as described above. After one week, tumor-bearing mice were injected intraperitoneally with 100 mg/kg tamoxifen (dissolved in corn oil at 20 mg/mL) per day for 5 consecutive days (day 8/9/10/11/12) to induce TiCas9 expression. Animals were euthanized according to university animal care guidelines upon the appearance of overt disease symptoms. For the *in vivo* competitive proliferation experiments, brain tissues were collected, dissociated with

the Worthington Papain Dissociation System (LK003150) according to the manufacturer's protocol, and analyzed by flow cytometry.

CRISPR sgRNA library composition—For the CRISPR screen, we assembled an sgRNA library consisting of a total of 4620 unique sgRNAs, which included personalized recurrent GBM-specific sgRNAs, personalized cancer-specific repeat sgRNAs, positive controls (e.g., sgCIDEs), and negative controls (e.g., non-targeting sgRNAs). All cancer-specific guide RNA sets contain sgRNAs that are specific for the recurrent hypermutated GBM PDCL SF11411 (sequencing replicate 1 and 2). For the oligo pool (60-mers, Twist Bioscience), some sgRNAs were included multiple times for better representation (4965 oligos total, Table S3).

Concretely, the CRISPR library contained the following sets of sgRNAs: 1) Previously tested sgCIDEs. 2) Non-targeting sgRNAs. This set contains 80 sgRNAs that have no exact target or positional off-target up to Hamming Distance (HD) 3 in the human genome. 3) Safe-harbor sgRNAs. A set of 1000 safe-harbor sgRNAs that are specific to their single target site in the human genome and have no off-targets up to HD 3 in the hg38 assembly. 4) Cancer-specific gene targeting sgRNAs. The "all-genes" set contains SF11411-specific, curated sgRNAs that target coding exons in the human genome. There are 1463 genes with 3165 sgRNAs. The "essentialgenes" set is a subset of all-genes with sgRNAs that target known essential genes. There are 41 genes with 67 sgRNAs. 5) Cancer-specific MYC transcription factor binding site (TFBS) targeting sgRNAs. The "MYC-TFBS" set contains sgRNAs targeting MYC transcription factor binding sites (Encode 3). There are 95 MYC TFBS with 183 sgRNAs. 6) Cancer-specific CTCF targeting sgRNAs. The "CTCF" set contains sgRNAs targeting CCCTC-binding factor (CTCF) sites. There are 7 CTCF sites with 12 gRNAs. 7) Cancer-specific vista enhancer targeting sgRNAs. The "vista-enhancer" set contains sgRNAs targeting highly conserved vista enhancers. There are 83 vista enhancers with 130 sgRNAs. 8) Cancer-specific sgRNAs targeting repetitive sequences. The "cancer duplicate (a.k.a. cancer repeat)" set contains sgRNAs that are a) repetitive in the recurrent cancer and b) unique to the recurrent cancer. There are 10 cancer repeat sgRNAs that meet these criteria. The most repetitive sgRNA has 7 enumerated repeats at HD 0.

Pooled sgRNA library generation and lentivirus production—A pooled oligo library was synthesized (Twist Bioscience) and then PCR amplified using primers Amp_fw cttgtggaaaggacgaaacaccg and Amp_rv gctatgctgtttccagcatagctc. The sgRNA inserts were then ligated into digested pCF822 backbone at a 5:1 ratio via Gibson Assembly (NEB #E2611). The recombinant plasmids were precipitated with isopropanol and electroporated into Endura ElectroCompetent cells (Lucigen #60242). The cells were plated onto LB agar 245-mm square bioassay dishes (Corning #31111) supplemented with ampicillin (100 μg/mL) for 12–14 h at 37°C. The colonies were harvested and plasmid DNA was extracted using the Qiagen Plasmid Maxi Kit (Qiagen #12163). To confirm the sgRNA distribution of the pooled library, an amplicon library containing the sgRNA cassettes was generated using NEBNext Ultra II Q5 Master Mix (NEB# M0544). The first step PCR primers contain partial Illumina adaptors: NGS_fw

ACACTCTTTCCCTACACGACGCTCTTCCGATCTggactatcatatgcttaccg, and NGS_rv GTGACTGGAGTTCAGACGTGTGCTCTTCCGATCTggtgccacttttttcaagttg. A second PCR was performed to attach Illumina adaptors and to barcode samples. The amplicon library was then sequenced on Illumina platforms with at least 100x coverage.

To produce lentivirus, HEK293FT cells were seeded at ~75% confluency the day before transfection in a 10 cm plate containing 8 mL of DMEM with 10% FBS and 1% penicillin/streptomycin. Transfection was performed by mixing 14 μg of DNA (8 μg sgRNA library, 4 μg psPAX2, 2 μg pMD2.G) and 42 μg of PEI in 2 mL of Opti-MEM medium for each 10cm plate. The mixture was incubated for 25 min at room temperature before being added to cells. 24 h post-transfection, the medium was changed to 5 mL of serum-free DMEM/F12 medium. 48 h post-transfection, the virus was harvested and filtered through a 0.45 μm syringe filter. Aliquots were stored at −80°C.

CRISPR screen—SF11411 and NHA cells were transduced with our pooled sgRNA library at a MOI <0.3. Sufficient cells were transduced to achieve a presentation of at least 2000 cells per sgRNA. One day post-transduction, half of the cells were collected for genomic DNA (gDNA) extraction (T0 samples) using the Quick-DNA Miniprep Plus Kit (Zymo Research #D4068). Two days after transduction, puromycin (2 μg/mL) was added to the cells for selection. Throughout the screen, cells were split at a density to maintain a representation of at least 1000 cells per sgRNA, and cell count was performed to monitor cell growth.

Four weeks post-transduction (~14 cell doubling), cells were collected for gDNA extraction using the same kit mentioned above. sgRNA cassettes were PCR amplified following the protocol described earlier. The amplicon library was then sequenced on Illumina platforms with at least 500x coverage. The screen analysis was performed using MAGeCK.[62]

Computational quantification of sgCIDE targets—Reference genomes for the hg38, mm10, and galGal6 assemblies of the human, mouse, and chicken genomes were downloaded from the UCSC genome browser. FASTA files were extracted and the GuideScan software[68] was utilized to determine the identity, coordinates, and target occurrences of sgRNAs in the SpyCas9 CRISPR system.

Variant calling—Variant calling was conducted using the Mutect2 application from the GATK software.[26] Variant calling was done on whole genome sequencing data of the patient's wildtype, primary cancer, and recurrent cancer genome. As the whole genome sequencing data was computed in the hg19 assembly of the human genome, variant calling with Mutect2 also used the hg19 assembly as its reference. Variants called in the primary and recurrent tumors were filtered against the variants in the patient's native genome, resulting in a list of cancer specific variants. Variant coordinates were assessed against coordinates of human exons in protein coding genes. If a variant coordinate overlapped an exon in a protein coding gene, the variant was labeled a coding variant. If the variant did not overlap an exon, then the variant was labeled non-coding.

Suspected pathogenic variants—To identify variants that are likely pathogenic, the identified patient native genome, patient primary GBM, and patient recurrent GBM variants were intersected with the ClinVar (NCBI) database (accessed 7/19/2022: https://ftp.ncbi.nlm.nih.gov/pub/clinvar/vcf_GRCh37/clinvar.vcf.gz). Specifically, we assessed whether patient-specific variants had a coordinate match with variants noted in ClinVar; however, we did not require that the identity of the mutation in our data matches the exact mutation reported in ClinVar. As possibly pathogenic, we considered ClinVar entries from the following categories: Pathogenic, Likely_pathogenic, risk_factor, Pathogenic/Likely_pathogenic, Pathogenic|_risk_factor, and Conflicting_interpretations_of_pathogenicity for cases where the majority of the reported studies support the variant being pathogenic/likely_pathogenic/risk_factor.

Determination of cancer specific sgRNAs—Variants were computed using Mutect2 from the GATK software.[26] Variants passing a threshold of 6.3 TLOD score were deemed to be variants of high confidence. These variants were compared against coordinates of genetic features of interest. Coordinates of overlapping features had sgRNAs computed from the variant. The sgRNAs from the variant were assessed against known sgRNAs in the human genome to determine if resulting sgRNA were specific to the cancer. An analysis of the variants to verify the TMZ chemotherapy signature was done with custom python scripts that processed the output files of the Mutect2 software.

Circos plots—Circos plots were generated using the Circa software (OMGenomics). Input files for circos plots were generated from sgRNA genomic coordinates that were determined using the GuideScan[68] software.

QUANTIFICATION AND STATISTICAL ANALYSIS

Statistical analyses were performed using Prism (GraphPad), Excel (Microsoft), and SciPy (version 1.6.2) software. Quantified data represent mean ± standard deviation (SD), unless otherwise indicated. Values of “n” are listed in relevant methods and/or figure legends. Multiple hypothesis testing correction was computed using the Benjamini-Hochberg procedure. Non-parametric statistical tests (e.g., Wilcoxon Rank Sum) were used in instances where the underlying distribution of study was unknown or unlikely to follow Gaussian behavior.

Supplementary Material

Refer to Web version on PubMed Central for supplementary material.

ACKNOWLEDGMENTS

We are deeply thankful to Jennifer Clarke (UCSF) and Ivan Smirnov (UCSF) for providing patient and tumor whole-genome sequencing (WGS) data. We thank David Raleigh, Tomoko Ozawa, and Kyounghee Seo from the UCSF Brain Tumor Center Preclinical Therapeutics Core for providing GL261 mouse GBM cells and the SF11411 patient-derived cell line (PDCL). This work was supported by NIH/NIGMS Pathway to Independence Award K99/R00 GM118909 (C.F.), NIH/NIGMS Maximizing Investigators’ Research Award (MIRA) for ESI R35 GM143124 (C.F.), a UCSF Brain Tumor SPORE CEP Award (C.F.), a UCSF Brain Tumor SPORE DRP Award (C.F.), and a generous gift from the UCSF Fishgold Hurwitt Brain Tumor Research Fund (C.F. and J.A.D.). J.A.D. is a Howard Hughes Medical Institute (HHMI) investigator. We thank J.A.D. and C.F. lab members for insightful comments and discussions.

REFERENCES

1. Louis DN, Perry A, Reifenberger G, von Deimling A, Figarella-Branger D, Cavenee WK, Ohgaki H, Wiestler OD, Kleihues P, and Ellison DW (2016). The 2016 World Health Organization Classification of Tumors of the Central Nervous System: a summary. Acta Neuropathol. 131, 803–820. 10.1007/s00401-016-1545-1. [PubMed: 27157931]
2. Stupp R, Mason WP, van den Bent MJ, Weller M, Fisher B, Taphoorn MJB, Belanger K, Brandes AA, Marosi C, Bogdahn U, et al. (2005). Radiotherapy plus concomitant and adjuvant temozolomide for glioblastoma. N. Engl. J. Med. 352, 987–996. 10.1056/NEJMoa043330. [PubMed: 15758009]
3. van Solinge TS, Nieland L, Chiocca EA, and Broekman MLD (2022). Advances in local therapy for glioblastoma - taking the fight to the tumour. Nat. Rev. Neurol. 18, 221–236. 10.1038/s41582-022-00621-0. [PubMed: 35277681]
4. Qazi MA, Vora P, Venugopal C, Sidhu SS, Moffat J, Swanton C, and Singh SK (2017). Intratumoral heterogeneity: pathways to treatment resistance and relapse in human glioblastoma. Ann. Oncol. 28, 1448–1456. 10.1093/annonc/mdx169. [PubMed: 28407030]
5. Neftel C, Laffy J, Filbin MG, Hara T, Shore ME, Rahme GJ, Richman AR, Silverbush D, Shaw ML, Hebert CM, et al. (2019). An Integrative Model of Cellular States, Plasticity, and Genetics for Glioblastoma. Cell 178, 835–849.e21. 10.1016/j.cell.2019.06.024. [PubMed: 31327527]
6. Patel AP, Tirosh I, Trombetta JJ, Shalek AK, Gillespie SM, Wakimoto H, Cahill DP, Nahed BV, Curry WT, Martuza RL, et al. (2014). Single-cell RNA-seq highlights intratumoral heterogeneity in primary glioblastoma. Science 344, 1396–1401. 10.1126/science.1254257. [PubMed: 24925914]
7. Johnson BE, Mazor T, Hong C, Barnes M, Aihara K, McLean CY, Fouse SD, Yamamoto S, Ueda H, Tatsuno K, et al. (2014). Mutational analysis reveals the origin and therapy-driven evolution of recurrent glioma. Science 343, 189–193. 10.1126/science.1239947. [PubMed: 24336570]
8. Hegi ME, Diserens A-C, Gorlia T, Hamou M-F, de Tribolet N, Weller M, Kros JM, Hainfellner JA, Mason W, Mariani L, et al. (2005). MGMT gene silencing and benefit from temozolomide in glioblastoma. N. Engl. J. Med. 352, 997–1003. 10.1056/NEJMoa043331. [PubMed: 15758010]
9. Lee SY (2016). Temozolomide resistance in glioblastoma multiforme. Genes Dis. 3, 198–210. 10.1016/j.gendis.2016.04.007. [PubMed: 30258889]
10. Touat M, Li YY, Boynton AN, Spurr LF, Iorgulescu JB, Bohrson CL, Cortes-Ciriano I, Birzu C, Geduldig JE, Pelton K, et al. (2020). Mechanisms and therapeutic implications of hypermutation in gliomas. Nature 580, 517–523. 10.1038/s41586-020-2209-9. [PubMed: 32322066]
11. Alexandrov LB, Nik-Zainal S, Wedge DC, Aparicio SAJR, Behjati S, Biankin AV, Bignell GR, Bolli N, Borg A, Børresen-Dale AL, et al. (2013). Signatures of mutational processes in human cancer. Nature 500, 415–421. 10.1038/nature12477. [PubMed: 23945592]
12. Jinek M, Chylinski K, Fonfara I, Hauer M, Doudna JA, and Charpentier E (2012). A programmable dual-RNA-guided DNA endonuclease in adaptive bacterial immunity. Science (1979) 337, 816–821, [pii]. 10.1126/science.1225829science.1225829.
13. Jinek M, East A, Cheng A, Lin S, Ma E, and Doudna J (2013). RNA-programmed genome editing in human cells. Elife 2, e00471. 10.7554/eLife.00471. [PubMed: 23386978]
14. Mali P, Yang L, Esvelt KM, Aach J, Guell M, DiCarlo JE, Norville JE, and Church GM (2013). RNA-guided human genome engineering via Cas9. Science 339, 823–826. 10.1126/science.1232033. [PubMed: 23287722]
15. Miller JC, Holmes MC, Wang J, Guschin DY, Lee Y-L, Rupniewski I, Beausejour CM, Waite AJ, Wang NS, Kim KA, et al. (2007). An improved zinc-finger nuclease architecture for highly specific genome editing. Nat. Biotechnol. 25, 778–785. 10.1038/nbt1319. [PubMed: 17603475]
16. Cho SW, Kim S, Kim JM, and Kim J-S (2013). Targeted genome engineering in human cells with the Cas9 RNA-guided endonuclease. Nat. Biotechnol. 31, 230–232. 10.1038/nbt.2507. [PubMed: 23360966]
17. Fellmann C, Gowen BG, Lin P-C, Doudna JA, and Corn JE (2017). Cornerstones of CRISPR-Cas in drug discovery and therapy. Nat. Rev. Drug Discov. 16, 89–100. 10.1038/nrd.2016.238. [PubMed: 28008168]

18. Leibowitz ML, Papathanasiou S, Doerfler PA, Blaine LJ, Sun L, Yao Y, Zhang C-Z, Weiss MJ, and Pellman D (2021). Chromothripsis as an on-target consequence of CRISPR–Cas9 genome editing. Nat. Genet. 53, 895–905. 10.1038/s41588-021-00838-7. [PubMed: 33846636]
19. Ihry RJ, Worringer KA, Salick MR, Frias E, Ho D, Theriault K, Kommineni S, Chen J, Sondey M, Ye C, et al. (2018). p53 inhibits CRISPR-Cas9 engineering in human pluripotent stem cells. Nat. Med. 24, 939–946. 10.1038/s41591-018-0050-6. [PubMed: 29892062]
20. Aguirre AJ, Meyers RM, Weir BA, Vazquez F, Zhang C-Z, Ben-David U, Cook A, Ha G, Harrington WF, Doshi MB, et al. (2016). Genomic Copy Number Dictates a Gene-Independent Cell Response to CRISPR/Cas9 Targeting. Cancer Discov. 6, 914–929. 10.1158/2159-8290.CD-16-0154. [PubMed: 27260156]
21. Wang T, Birsoy K, Hughes NW, Krupczak KM, Post Y, Wei JJ, Lander ES, and Sabatini DM (2015). Identification and characterization of essential genes in the human genome. Science 350, 1096–1101. 10.1126/science.aac7041. [PubMed: 26472758]
22. Munoz DM, Cassiani PJ, Li L, Billy E, Korn JM, Jones MD, Golji J, Ruddy DA, Yu K, McAllister G, et al. (2016). CRISPR Screens Provide a Comprehensive Assessment of Cancer Vulnerabilities but Generate False-Positive Hits for Highly Amplified Genomic Regions. Cancer Discov. 6, 900–913. 10.1158/2159-8290.CD-16-0178. [PubMed: 27260157]
23. Yang L, Güell M, Niu D, George H, Lesha E, Grishin D, Aach J, Shrock E, Xu W, Poci J, et al. (2015). Genome-wide inactivation of porcine endogenous retroviruses (PERVs). Science 350, 1101–1104. 10.1126/science.aad1191. [PubMed: 26456528]
24. Niu D, Wei H-J, Lin L, George H, Wang T, Lee I-H, Zhao H-Y, Wang Y, Kan Y, Shrock E, et al. (2017). Inactivation of porcine endogenous retrovirus in pigs using CRISPR-Cas9. Science 357, 1303–1307. 10.1126/science.aan4187. [PubMed: 28798043]
25. Zehir A, Benayed R, Shah RH, Syed A, Middha S, Kim HR, Srinivasan P, Gao J, Chakravarty D, Devlin SM, et al. (2017). Mutational landscape of metastatic cancer revealed from prospective clinical sequencing of 10,000 patients. Nat. Med. 23, 703–713. 10.1038/nm.4333. [PubMed: 28481359]
26. McKenna A, Hanna M, Banks E, Sivachenko A, Cibulskis K, Kernytsky A, Garimella K, Altshuler D, Gabriel S, Daly M, and DePristo MA (2010). The Genome Analysis Toolkit: a MapReduce framework for analyzing next-generation DNA sequencing data. Genome Res. 20, 1297–1303. 10.1101/gr.107524.110. [PubMed: 20644199]
27. Venter JC, Adams MD, Myers EW, Li PW, Mural RJ, Sutton GG, Smith HO, Yandell M, Evans CA, Holt RA, et al. (2001). The sequence of the human genome. Science 291, 1304–1351. 10.1126/science.1058040. [PubMed: 11181995]
28. 1000 Genomes Project Consortium; Auton A, Brooks LD, Durbin RM, Garrison EP, Kang HM, Korbel JO, Marchini JL, McCarthy S, McVean GA, and Abecasis GR (2015). A global reference for human genetic variation. Nature 526, 68–74. 10.1038/nature15393. [PubMed: 26432245]
29. Lander ES, Linton LM, Birren B, Nusbaum C, Zody MC, Baldwin J, Devon K, Dewar K, Doyle M, FitzHugh W, et al. (2001). Initial sequencing and analysis of the human genome. Nature 409, 860–921. 10.1038/35057062. [PubMed: 11237011]
30. Bartek J, and Lukas J (2003). Chk1 and Chk2 kinases in checkpoint control and cancer. Cancer Cell 3, 421–429. 10.1016/s1535-6108(03)00110-7. [PubMed: 12781359]
31. Zannini L, Delia D, and Buscemi G (2014). CHK2 kinase in the DNA damage response and beyond. J. Mol. Cell Biol. 6, 442–457. 10.1093/jmcb/mju045.
32. Squatrito M, Brennan CW, Helmy K, Huse JT, Petrini JH, and Holland EC (2010). Loss of ATM/Chk2/p53 pathway components accelerates tumor development and contributes to radiation resistance in gliomas. Cancer Cell 18, 619–629. 10.1016/j.ccr.2010.10.034. [PubMed: 21156285]
33. Shaag A, Walsh T, Renbaum P, Kirchhoff T, Nafa K, Shiovitz S, Mandell JB, Welcsh P, Lee MK, Ellis N, et al. (2005). Functional and genomic approaches reveal an ancient CHEK2 allele associated with breast cancer in the Ashkenazi Jewish population. Hum. Mol. Genet. 14, 555–563. 10.1093/hmg/ddi052. [PubMed: 15649950]
34. Adamson AW, Beardsley DI, Kim W-J, Gao Y, Baskaran R, and Brown KD (2005). Methylator-induced, mismatch repair-dependent G2 arrest is activated through Chk1 and Chk2. Mol. Biol. Cell 16, 1513–1526. 10.1091/mbc.e04-02-0089. [PubMed: 15647386]

35. Watanabe R, Ui A, Kanno S-I, Ogiwara H, Nagase T, Kohno T, and Yasui A (2014). SWI/SNF factors required for cellular resistance to DNA damage include ARID1A and ARID1B and show interdependent protein stability. Cancer Res. 74, 2465–2475. 10.1158/0008-5472.CAN-13-3608. [PubMed: 24788099]

36. Ichimura K, Mungall AJ, Fiegler H, Pearson DM, Dunham I, Carter NP, and Collins VP (2006). Small regions of overlapping deletions on 6q26 in human astrocytic tumours identified using chromosome 6 tile path array-CGH. Oncogene 25, 1261–1271. 10.1038/sj.onc.1209156. [PubMed: 16205629]

37. Sausen M, Leary RJ, Jones S, Wu J, Reynolds CP, Liu X, Blackford A, Parmigiani G, Diaz LA, Papadopoulos N, et al. (2013). Integrated genomic analyses identify ARID1A and ARID1B alterations in the childhood cancer neuroblastoma. Nat. Genet. 45, 12–17. 10.1038/ng.2493. [PubMed: 23202128]

38. Amen AM, Fellmann C, Soczek KM, Ren SM, Lew RJ, Knott GJ, Park JE, McKinney AM, Mancini A, Doudna JA, and Costello JF (2021). Cancer-specific loss of TERT activation sensitizes glioblastoma to DNA damage. Proc. Natl. Acad. Sci. USA 118, e2008772118. 10.1073/pnas.2008772118. [PubMed: 33758097]

39. Mancini A, Xavier-Magalhães A, Woods WS, Nguyen K-T, Amen AM, Hayes JL, Fellmann C, Gapinske M, McKinney AM, Hong C, et al. (2018). Disruption of the b1L Isoform of GABP Reverses Glioblastoma Replicative Immortality in a TERT Promoter Mutation-Dependent Manner. Cancer Cell 34, 513–528.e8. 10.1016/j.ccell.2018.08.003. [PubMed: 30205050]

40. Bell RJA, Rube HT, Kreig A, Mancini A, Fouse SD, Nagarajan RP, Choi S, Hong C, He D, Pekmezci M, et al. (2015). Cancer. The transcription factor GABP selectively binds and activates the mutant TERT promoter in cancer. Science 348, 1036–1039. 10.1126/science.aab0015. [PubMed: 25977370]

41. Killela PJ, Reitman ZJ, Jiao Y, Bettegowda C, Agrawal N, Diaz LA, Friedman AH, Friedman H, Gallia GL, Giovanella BC, et al. (2013). TERT promoter mutations occur frequently in gliomas and a subset of tumors derived from cells with low rates of self-renewal. Proc. Natl. Acad. Sci. USA 110, 6021–6026. 10.1073/pnas.1303607110. [PubMed: 23530248]

42. Horn S, Figl A, Rachakonda PS, Fischer C, Sucker A, Gast A, Kadel S, Moll I, Nagore E, Hemminki K, et al. (2013). TERT promoter mutations in familial and sporadic melanoma. Science 339, 959–961. 10.1126/science.1230062. [PubMed: 23348503]

43. Huang FW, Hodis E, Xu MJ, Kryukov GV, Chin L, and Garraway LA (2013). Highly recurrent TERT promoter mutations in human melanoma. Science 339, 957–959. 10.1126/science.1229259. [PubMed: 23348506]

44. AACR Project GENIE Consortium (2017). AACR Project GENIE: Powering Precision Medicine through an International Consortium. Cancer Discov. 7, 818–831. 10.1158/2159-8290.CD-17-0151. [PubMed: 28572459]

45. Oakes BL, Fellmann C, Rishi H, Taylor KL, Ren SM, Nadler DC, Yokoo R, Arkin AP, Doudna JA, and Savage DF (2019). CRISPR-Cas9 Circular Permutants as Programmable Scaffolds for Genome Modification. Cell 176, 254–267.e16. 10.1016/j.cell.2018.11.052. [PubMed: 30633905]

46. Ellegren H (2004). Microsatellites: simple sequences with complex evolution. Nat. Rev. Genet. 5, 435–445. 10.1038/nrg1348. [PubMed: 15153996]

47. Furey TS, and Haussler D (2003). Integration of the cytogenetic map with the draft human genome sequence. Hum. Mol. Genet. 12, 1037–1044. 10.1093/hmg/ddg113. [PubMed: 12700172]

48. Hart T, Brown KR, Sircoulomb F, Rottapel R, and Moffat J (2014). Measuring error rates in genomic perturbation screens: gold standards for human functional genomics. Mol. Syst. Biol. 10, 733. [PubMed: 24987113]

49. Pegg AE, Wiest L, Foote RS, Mitra S, and Perry W (1983). Purification and properties of O6-methylguanine-DNA transmethylase from rat liver. J. Biol. Chem. 258, 2327–2333. [PubMed: 6822564]

50. Hirose Y, Berger MS, and Pieper RO (2001). p53 effects both the duration of G2/M arrest and the fate of temozolomide-treated human glioblastoma cells. Cancer Res. 61, 1957–1963. [PubMed: 11280752]

51. Baugh EH, Ke H, Levine AJ, Bonneau RA, and Chan CS (2018). Why are there hotspot mutations in the TP53 gene in human cancers? Cell Death Differ. 25, 154–160. 10.1038/cdd.2017.180. [PubMed: 29099487]
52. Watters KE, Fellmann C, Bai HB, Ren SM, and Doudna JA (2018). Systematic discovery of natural CRISPR-Cas12a inhibitors. Science 362, 236–239. 10.1126/science.aau5138. [PubMed: 30190307]
53. Jiang W, Bikard D, Cox D, Zhang F, and Marraffini LA (2013). RNA-guided editing of bacterial genomes using CRISPR-Cas systems. Nat. Biotechnol. 31, 233–239. 10.1038/nbt.2508. [PubMed: 23360965]
54. Oakes BL, Nadler DC, Flamholz A, Fellmann C, Staahl BT, Doudna JA, and Savage DF (2016). Profiling of engineering hotspots identifies an allosteric CRISPR-Cas9 switch. Nat. Biotechnol. 34, 646–651. 10.1038/nbt.3528. [PubMed: 27136077]
55. Doench JG, Fusi N, Sullender M, Hegde M, Vaimberg EW, Donovan KF, Smith I, Tothova Z, Wilen C, Orchard R, et al. (2016). Optimized sgRNA design to maximize activity and minimize off-target effects of CRISPR-Cas9. Nat. Biotechnol. 34, 184–191. 10.1038/nbt.3437. [PubMed: 26780180]
56. Fu Y, Foden JA, Khayter C, Maeder ML, Reyon D, Joung JK, and Sander JD (2013). High-frequency off-target mutagenesis induced by CRISPR-Cas nucleases in human cells. Nat. Biotechnol. 31, 822–826. 10.1038/nbt.2623. [PubMed: 23792628]
57. Hsu PD, Scott DA, Weinstein JA, Ran FA, Konermann S, Agarwala V, Li Y, Fine EJ, Wu X, Shalem O, et al. (2013). DNA targeting specificity of RNA-guided Cas9 nucleases. Nat. Biotechnol. 31, 827–832. 10.1038/nbt.2647. [PubMed: 23873081]
58. Yarrington RM, Verma S, Schwartz S, Trautman JK, and Carroll D (2018). Nucleosomes inhibit target cleavage by CRISPR-Cas9 in vivo. Proc. Natl. Acad. Sci. USA 115, 9351–9358. 10.1073/pnas.1810062115. [PubMed: 30201707]
59. Jensen KT, Fløe L, Petersen TS, Huang J, Xu F, Bolund L, Luo Y, and Lin L (2017). Chromatin accessibility and guide sequence secondary structure affect CRISPR-Cas9 gene editing efficiency. FEBS Lett. 591, 1892–1901. 10.1002/1873-3468.12707. [PubMed: 28580607]
60. Zhao H, Thienpont B, Yesilyurt BT, Moisse M, Reumers J, Coenegrachts L, Sagaert X, Schrauwen S, Smeets D, Matthijs G, et al. (2014). Mismatch repair deficiency endows tumors with a unique mutation signature and sensitivity to DNA double-strand breaks. Elife 3, e02725. 10.7554/eLife.02725. [PubMed: 25085081]
61. Alexandrov LB, Kim J, Haradhvala NJ, Huang MN, Tian Ng AW, Wu Y, Boot A, Covington KR, Gordenin DA, Bergstrom EN, et al. (2020). The repertoire of mutational signatures in human cancer. Nature 578, 94–101. 10.1038/s41586-020-1943-3. [PubMed: 32025018]
62. Li W, Xu H, Xiao T, Cong L, Love MI, Zhang F, Irizarry RA, Liu JS, Brown M, and Liu XS (2014). MAGeCK enables robust identification of essential genes from genome-scale CRISPR/Cas9 knockout screens. Genome Biol. 15, 554. 10.1186/s13059-014-0554-4. [PubMed: 25476604]
63. Jones LE, Hilz S, Grimmer MR, Mazor T, Najac C, Mukherjee J, McKinney A, Chow T, Pieper RO, Ronen SM, et al. (2020). Patient-derived cells from recurrent tumors that model the evolution of IDH-mutant glioma. Neurooncol. Adv. 2, vdaa088. 10.1093/noajnl/vdaa088. [PubMed: 32904945]
64. Martínez-Jiménez F, Muiños F, Sentís I, Deu-Pons J, Reyes-Salazar I, Arnedo-Pac C, Mularoni L, Pich O, Bonet J, Kranas H, et al. (2020). A compendium of mutational cancer driver genes. Nat. Rev. Cancer 20, 555–572. 10.1038/s41568-020-0290-x. [PubMed: 32778778]
65. Wang Q, Liu X, Zhou J, Yang C, Wang G, Tan Y, Wu Y, Zhang S, Yi K, and Kang C (2019). The CRISPR-Cas13a Gene-Editing System Induces Collateral Cleavage of RNA in Glioma Cells. Adv. Sci. 6, 1901299. 10.1002/advs.201901299.
66. Davis JR, Banskota S, Levy JM, Newby GA, Wang X, Anzalone AV, Nelson AT, Chen PJ, Hennes AD, An M, et al. (2023). Efficient prime editing in mouse brain, liver and heart with dual AAVs. Nat. Biotechnol. 10.1038/s41587-023-01758-z.
67. Ohba S, Mukherjee J, Johannessen T-C, Mancini A, Chow TT, Wood M, Jones L, Mazor T, Marshall RE, Viswanath P, et al. (2016). Mutant IDH1 Expression Drives TERT Promoter

Reactivation as Part of the Cellular Transformation Process. Cancer Res. 76, 6680–6689. 10.1158/0008-5472.CAN-16-0696. [PubMed: 27758882]

68. Perez AR, Pritykin Y, Vidigal JA, Chhangawala S, Zamparo L, Leslie CS, and Ventura A (2017). GuideScan software for improved single and paired CRISPR guide RNA design. Nat. Biotechnol. 35, 347–349. 10.1038/nbt.3804. [PubMed: 28263296]
69. Mangeot PE, Risson V, Fusil F, Marnef A, Laurent E, Blin J, Mournetas V, Massouridè s E, Sohier TJM, Corbin A, et al. (2019). Genome editing in primary cells and in vivo using viral-derived Nanoblades loaded with Cas9-sgRNA ribonucleoproteins. Nat. Commun. 10, 45. 10.1038/s41467-018-07845-z. [PubMed: 30604748]
70. Amen AM, Loughran RM, Huang C-H, Lew RJ, Ravi A, Guan Y, Schatoff EM, Dow LE, Emerling BM, and Fellmann C (2022). Endogenous spacing enables co-processing of microRNAs and efficient combinatorial RNAi. Cell Rep. Methods 2, 100239. 10.1016/j.crmeth.2022.100239. [PubMed: 35880017]
71. Feil R, Wagner J, Metzger D, and Chambon P (1997). Regulation of Cre recombinase activity by mutated estrogen receptor ligand-binding domains. Biochem. Biophys. Res. Commun. 237, 752–757. 10.1006/bbrc.1997.7124. [PubMed: 9299439]
72. Buskirk AR, Ong Y-C, Gartner ZJ, and Liu DR (2004). Directed evolution of ligand dependence: small-molecule-activated protein splicing. Proc. Natl. Acad. Sci. USA 101, 10505–10510. 10.1073/pnas.0402762101. [PubMed: 15247421]
73. Watters KE, Shivram H, Fellmann C, Lew RJ, McMahon B, and Doudna JA (2020). Potent CRISPR-Cas9 inhibitors from Staphylococcus genomes. Proc. Natl. Acad. Sci. USA 117, 6531–6539. 10.1073/pnas.1917668117. [PubMed: 32156733]
74. Rauch BJ, Silvis MR, Hultquist JF, Waters CS, McGregor MJ, Krogan NJ, and Bondy-Denomy J (2017). Inhibition of CRISPR-Cas9 with Bacteriophage Proteins. Cell 168, 150–158.e10. 10.1016/j.cell.2016.12.009. [PubMed: 28041849]

Highlights

- CRISPR targeting of repetitive non-coding loci enables rapid glioma cell depletion
- Computation of patient data reveals personalized repeat sgRNAs in hypermutated GBM
- Unique repeat sequences are associated with TMZ mutational signature
- CRISPR targeting of cancer-specific repeats selectively ablates recurrent GBM

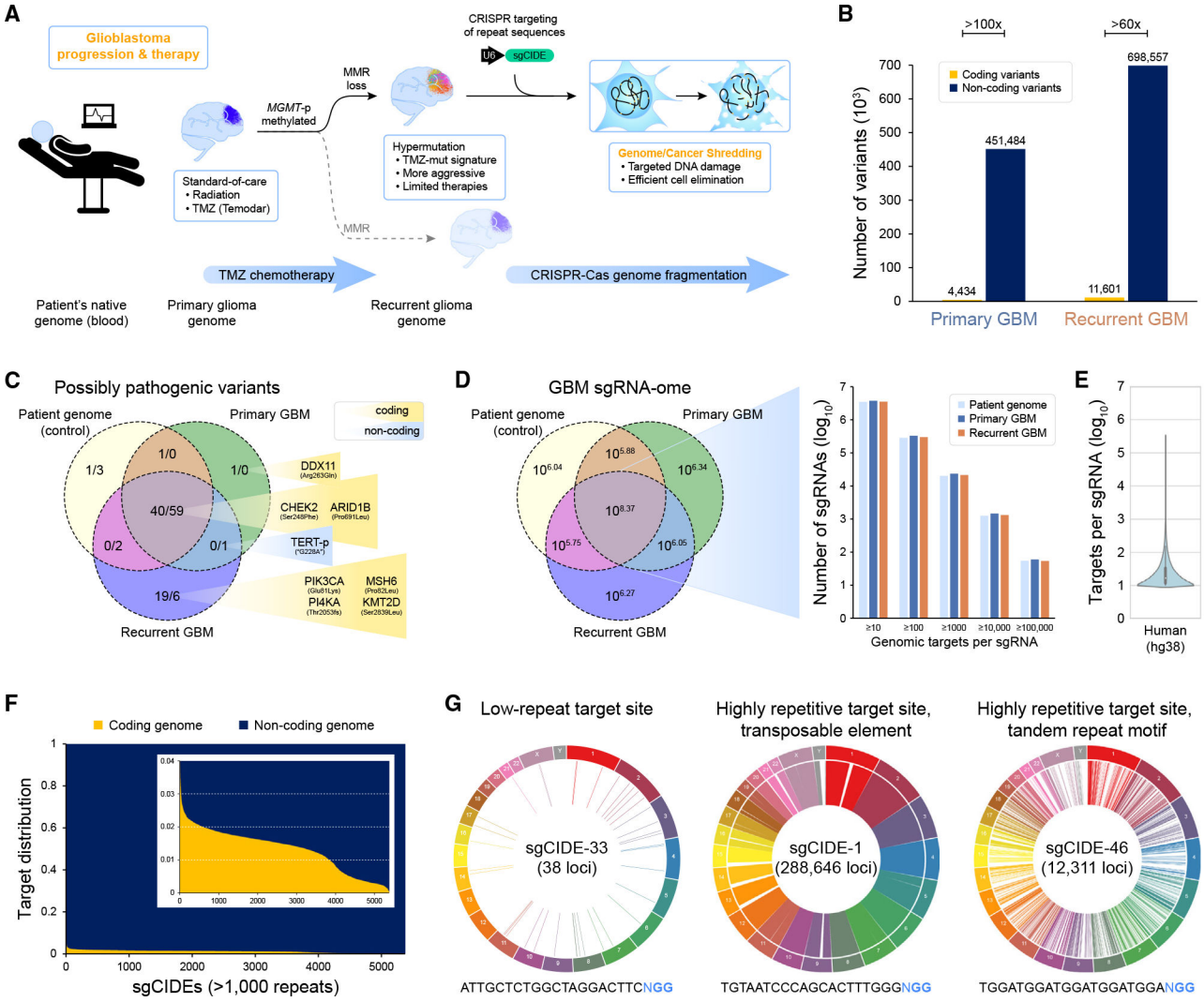

Figure 1. Glioma mutational landscape reveals non-coding genome as key source of variation

(A) Schematic of GBM progression with frontline therapy including radiation, TMZ chemotherapy, and surgical resection. Highlighted is CRISPR-Cas "genome/cancer shredding," a strategy for recurrent tumors that induces DNA damage and cell elimination through targeting of repetitive sequences in the genome. MMR, mismatch repair. *MGMT*-p, O-6-methylguanine-DNA methyltransferase promoter. sgCIDE, sgRNA targeting repeat loci.

(B) Quantification of protein-coding and non-coding variants (mutations) in a patient's primary and recurrent GBM compared to the patient's native genome. Variants were detected using Mutect2 based on whole-genome sequencing. Blood was used for the patient's native control.

(C) Venn diagram showing the patient's variants that are reported in ClinVar (NCBI) as risk factor, likely pathogenic, or pathogenic. Each section of the Venn diagram reports the number of coding and non-coding mutations (coding/non-coding).

(D) Venn diagram of the patient's collection of all possible sgRNAs, termed "sgRNA-ome." The right panel quantifies the number of sgRNAs with the indicated amount of repeat targets (20-mer sequences, 5′-NGG-3′ PAM).

(E) Violin plot of the repeat sgRNA-ome target counts in the human genome (hg38). Only sgRNAs with at least 10 target sites are represented.
(F) Target distribution of highly repetitive sgRNAs, termed “sgCIDE,” between coding and non-coding genome, showing repeat sgRNA mainly target the non-coding genome. The inlay shows a zoom-in, highlighting that there are two discrete key classes of sgCIDEs.
(G) Circos plots of select sgCIDEs indicating the location of target sites across the genome (Hamming distance = 0). Each line of the inner circle represents one target locus. The outer circle highlights the chromosomes.

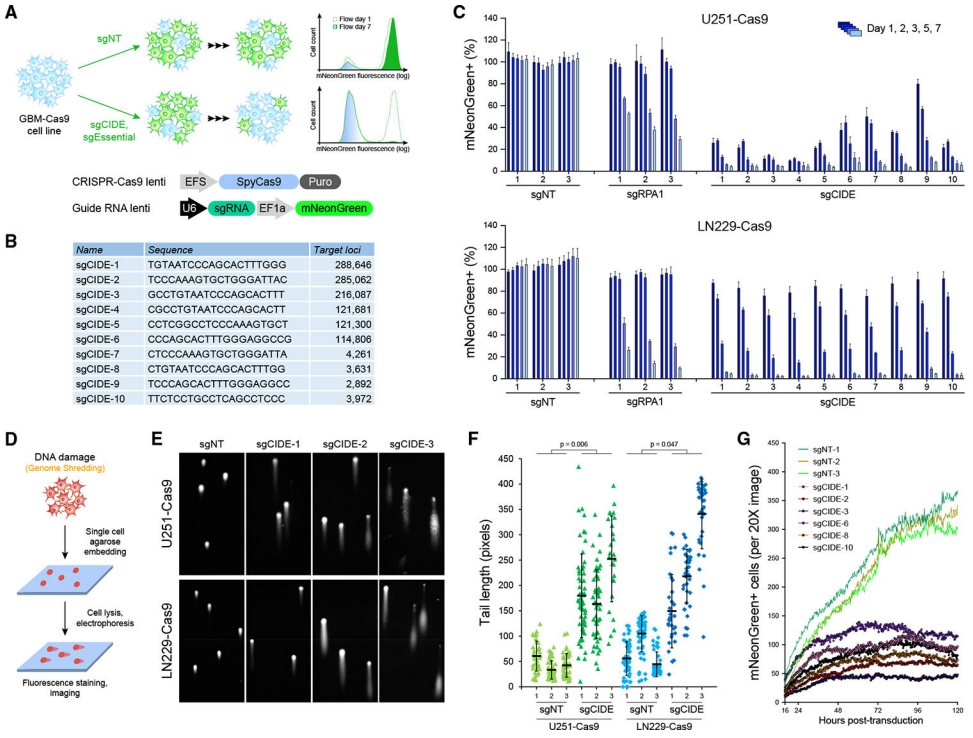

Figure 2. CRISPR-Cas genome shredding enables fast and efficient cell elimination

(A) Diagram of a competitive proliferation assay to quantify cell depletion rates using flow cytometry.

(B) Shown are the sgCIDE sequence and count of fully complementary (Hamming distance = 0) loci in the human genome.

(C) Competitive proliferation assay in Cas9-expressing U251 and LN229 GBM cells. Wild-type cells not expressing Cas9 were used for normalization. Cell lines were stably transduced with the indicated guide RNAs inducing genome shredding (sgCIDE), targeting an essential gene (sgRPA1), or representing a non-targeting control (sgNT). Changes in ratios of sgRNA-transduced cells (mNeonGreen+) were monitored by flow cytometry over 7 days. Error bars indicate SD (n = 3).

(D) Comet assay to assess genomic degradation at single-cell resolution.

(E) Comet assay demonstrating rapid and robust genome shredding at the single-cell level. Cas9-expressing U251 and LN229 cells were transduced with the indicated sgRNAs, and genome fragmentation was assessed at 24 h post transduction. Select representative images are shown.

(F) Quantification of genome fragmentation observed in comet assay in (E). Error bars indicate SD. Significance was determined using an unpaired, two-tailed t test.

(G) Genome shredding abolishes target cell proliferation. Growth curves showing the number of mNeonGreen+ cells detected by live-cell imaging of Cas9-expressing U251 transduced with the indicated sgRNAs. Quantification indicates the average count per condition across n = 4 images.

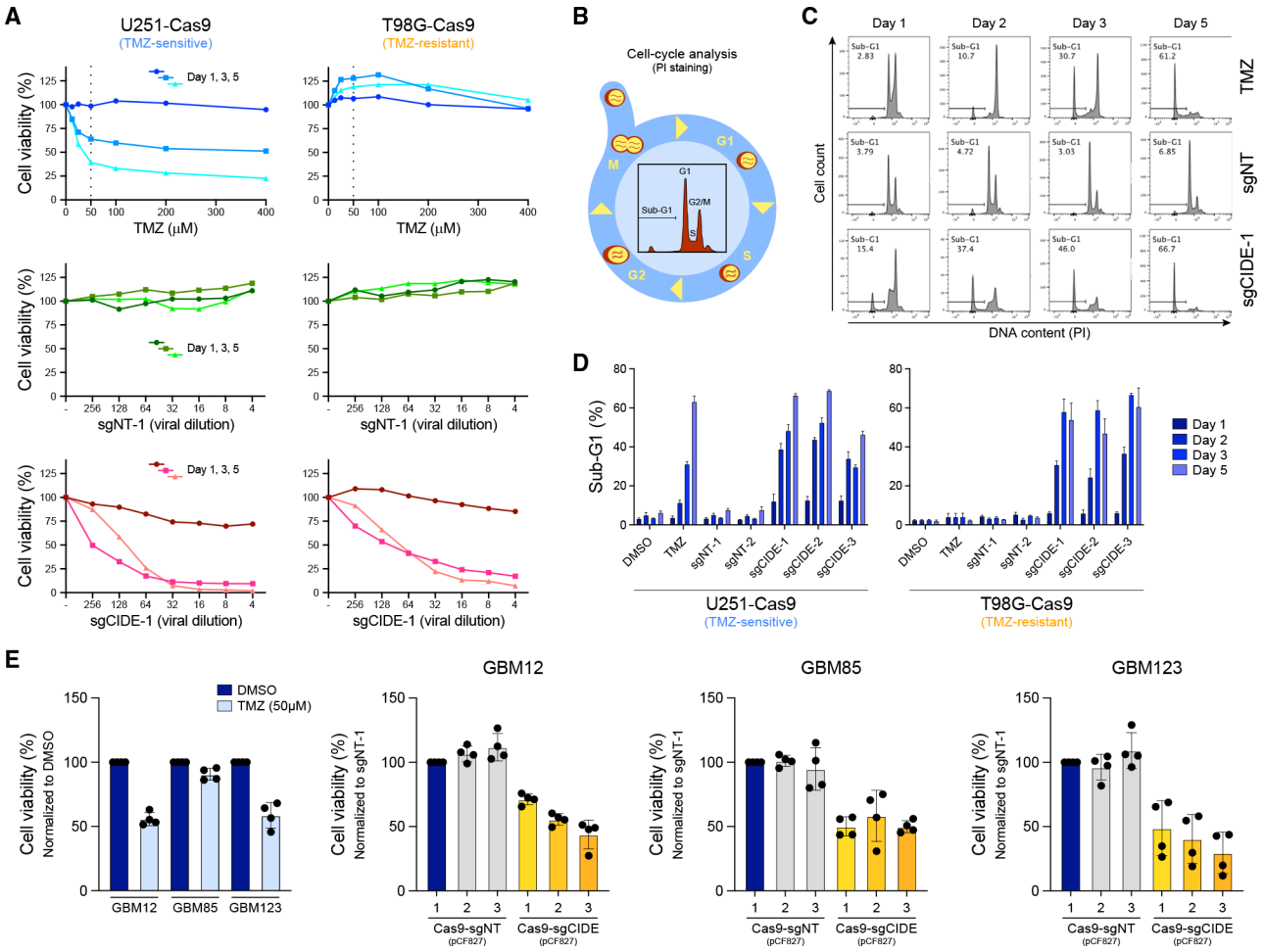

Figure 3. Genome shredding is cell-state agnostic and hard to escape

(A) Quantification of cell viability (CellTiter-Glo) after treatment of TMZ-sensitive and -resistant glioblastoma cells with TMZ (concentration gradient) or transduction with sgNTs and sgCIDEs (viral dilution gradient, 1:X).

(B) Schematic of cell-cycle analysis using flow cytometry. PI, propidium iodide.

(C) Cell-cycle analysis of TMZ- and sgCIDE-treated GBM cells. Cas9-expressing U251 cells were treated with TMZ (50 μM) or the indicated sgRNAs, and cell-cycle profiles analyzed after PI staining. Shown are select representative flow cytometry plots.

(D) Quantification of Sub-G1 fraction in cell-cycle profiles shown partially in (C). Cas9-expressing U251 and T98G cells were treated with DMSO, TMZ (50 μM), or the indicated sgRNAs and stained with PI after 1–5 days. Error bars indicate SD (n = 3).

(E) Quantification of cell viability 5 days after treating glioblastoma stem-like cells (GSCs) with TMZ (50 μM) or all-in-one lentiviral vectors (pCF827) to deliver Cas9 and sgRNAs (sgNT-1/2/3, sgCIDE-1/2/3). Error bars indicate SD (n = 4).

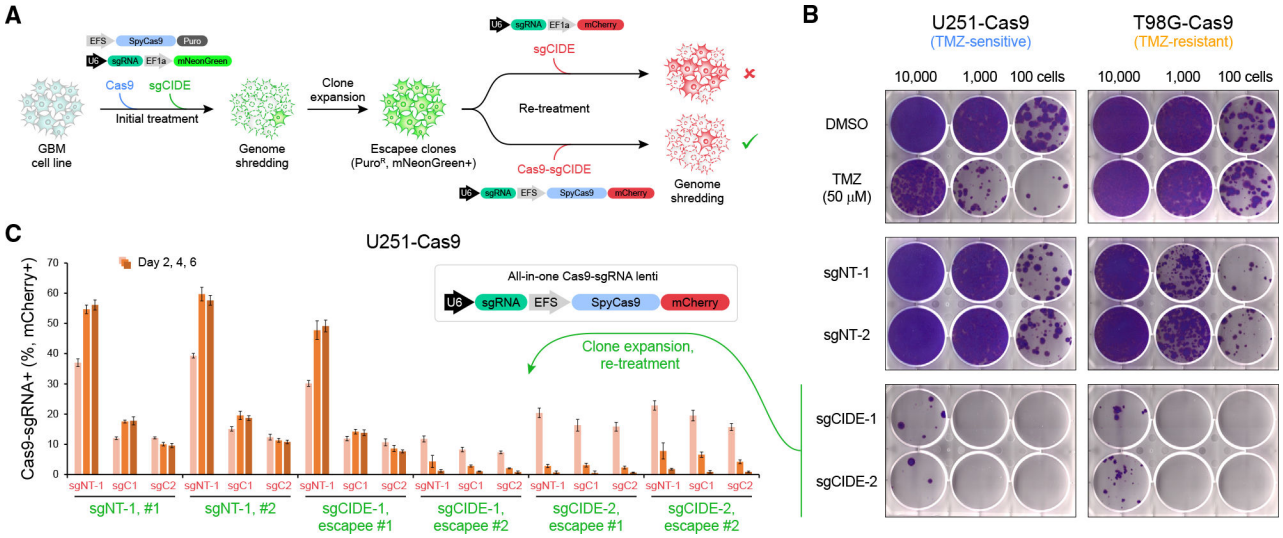

Figure 4. Rare escapee clones can efficiently be retreated

(A) Schematic showing retreatment of GBM cells that have escaped a first cycle of genome shredding. During initial treatment (colony formation assay), GBM cells are transduced with a lentiviral vector expressing Cas9 and a puromycin selection marker (pCF226), followed by a vector expressing an sgRNA and mNeonGreen (pCF821). Rare "escapee" cells that survive this regimen (Puro^R, mNeonGreen+) are expanded and treated a second time. Retreatment consists either of a vector expressing only an sgRNA and mCherry (pCF820) or an all-in-one vector expressing an sgRNA and Cas9 linked to an mCherry marker (pCF826).

(B) Colony formation assay in Cas9-expressing U251 and T98G.

(C) Quantification of cell depletion of the indicated U251-Cas9 escapee clones and controls treated with a vector (pCF826) expressing the indicated sgCIDE or sgNT-1 and Cas9 linked to mCherry. sgC1, sgCIDE-1. sgC2, sgCIDE-2. Error bars indicate SD (n = 3). Note, for three out of four escapee clones, re-expression of Cas9 alone was sufficient for cell depletion, indicating that the previously introduced sgCIDEs were still active in those clones.

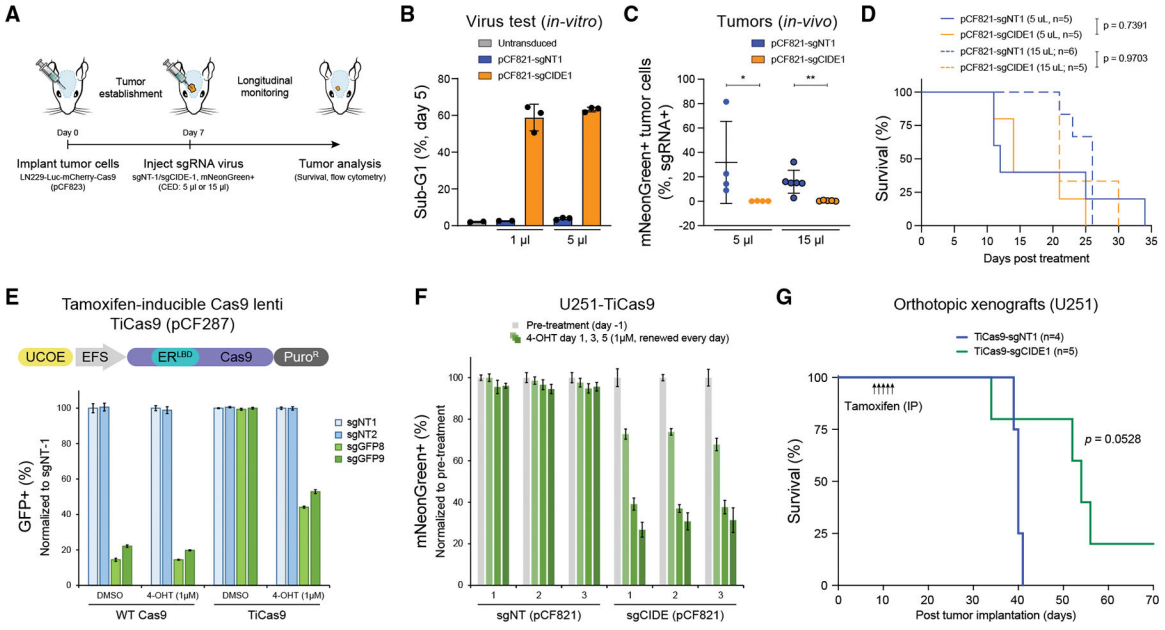

Figure 5. Genome shredding efficiently ablates GBM cells in vivo

(A) Representation of experimental design.

(B) Sub-G1 assay confirming that concentrated sgCIDE-1 virus efficiently transduces and destroys Cas9-expressing LN229 cells *in vitro*. Error bars indicate SD (n = 3).

(C) **In vivo** treatment of mice harboring Cas9-expressing LN229 GBM intracranial xenografts with sgRNA virus. Mouse brains were analyzed when tumor-related symptoms were observed. The percentage of mCherry+ (tumor cells) and mNeonGreen+ (sgRNA virus) cells from mice treated with 5 µL concentrated sgNT-1 or sgCIDE-1 virus (four mice each) and 15 µL concentrated sgNT-1 or sgCIDE-1 virus (six and five mice, respectively) were quantified by flow cytometry. Error bars indicate SD. Significance was determined using the Mann-Whitney test (*$p < 0.05$; **$p < 0.01$).

(D) Kaplan-Meier curves of mice harboring Cas9-expressing LN229 GBM intracranial xenografts treated with 5 µL or 15 µL concentrated sgNT-1 or sgCIDE-1 virus. Significance was determined using the log rank test.

(E) Flow cytometry analysis of wild-type (WT) Cas9 and TiCas9-edited HEK293T cells encoding GFP (HEK-RT1), demonstrating efficient inducible editing with TiCas9, though not fully matching WT Cas9. Error bars indicate SD (n = 3).

(F) Competitive proliferation assay in TiCas9-expressing U251 GBM cells. Untreated cells (pre-treatment) were used for normalization. Error bars indicate SD (n = 3).

(G) Kaplan-Meier curves of mice harboring TiCas9-sgRNA-expressing U251 GBM intracranial xenografts. Tumor-bearing mice were injected with tamoxifen for 5 consecutive days to induce TiCas9 expression 1 week after tumor implantation. Significance was determined using the log rank test.

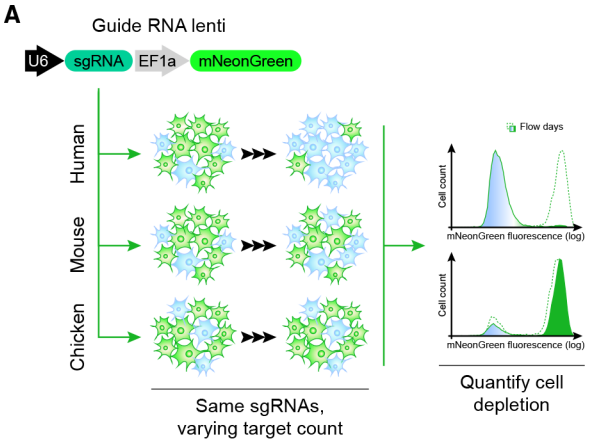

B

	Human targets		Mouse targets		Chicken targets	
Name	HD 0	HD 1	HD 0	HD 1	HD 0	HD 1
sgNT-1	0	0	0	0	0	0
sgNT-2	0	0	0	0	0	0
sgNT-3	0	0	0	0	0	0
sgCIDE-1	288646	280063	2	66	0	0
sgCIDE-2	285062	275253	2	70	0	0
sgCIDE-3	216087	280044	2	96	0	0
sgCIDE-31	1799	16658	3363	22649	0	0
sgCIDE-32	45	1554	123	3823	0	0
sgCIDE-33	38	1365	48	7480	0	0
sgCIDE-34	1186	5085	323	16925	0	0
sgCIDE-35	1125	3605	22202	8783	0	0
sgCIDE-36	20	1055	378	43050	0	0
sgCIDE-21	0	3	63328	49448	0	0
sgCIDE-22	0	0	137	45859	0	0
sgCIDE-23	0	0	45238	32216	0	0
sgCIDE-24	0	0	136	44675	0	0
sgCIDE-41	969	62884	3649	306606	293	19933
sgCIDE-42	1417	56409	13911	1308275	161	3908
sgCIDE-43	35034	28989	181654	57152	31858	5366
sgCIDE-44	216	32825	1785	193241	32	1493
sgCIDE-45	1792	17896	8516	76352	78	796
sgCIDE-46	12311	11853	22292	14433	3033	1858

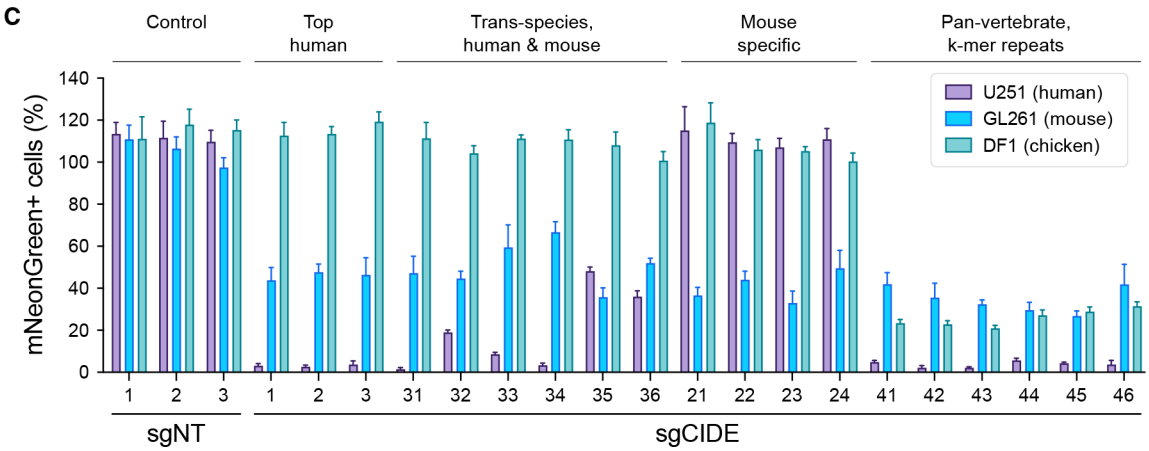

Figure 6. Minimal requirements for efficient cell ablation

(A) Competitive proliferation assays to evaluate CRISPR target requirements for efficient cell ablation by genome shredding in various eukaryotic cells.

(B) Target site occurrences for the indicated sgRNAs in the human (hg38), mouse (mm10), and chicken (galGal6) genomes. Quantified are the number of targets with full complementarity (HD 0) and one mismatch (HD 1). HD, Hamming distance (mismatches).

(C) Competitive proliferation assays in Cas9-expressing human (U251) and mouse (GL261) GBM cells and chicken fibroblasts (DF1). Wild-type cells not expressing Cas9 were used for normalization. Shown is the relative ratio of sgRNA-expressing (mNeonGreen+) cells at day 7 post transduction. Error bars indicate SD (n = 3).

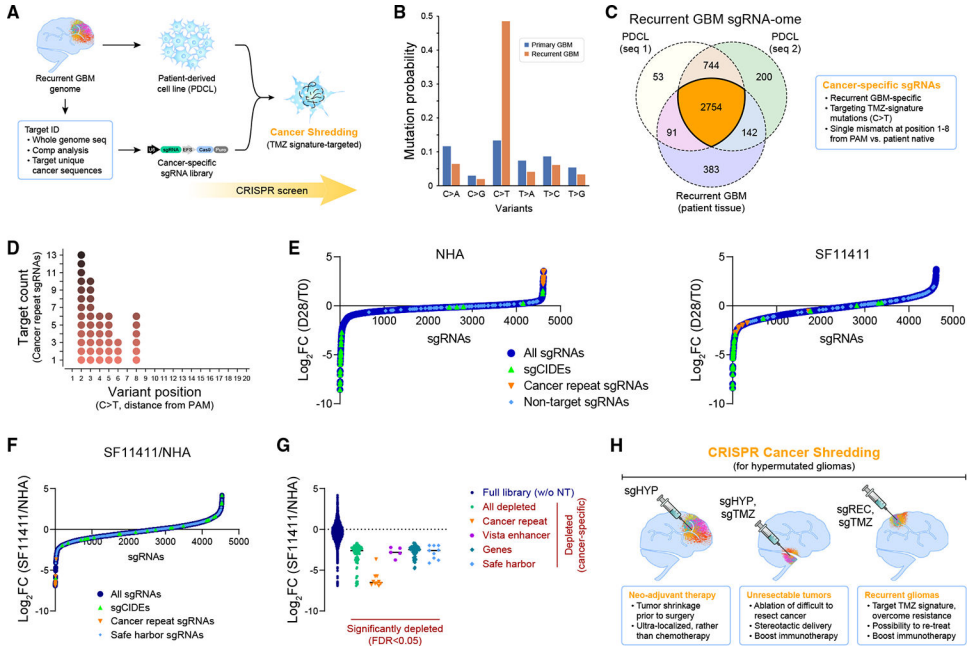

Figure 7. Targeting TMZ signature mutations enables selective elimination of recurrent GBM cells

(A) Diagram showing identification of cancer-specific sgRNAs and assessment of cancer shredding in a patient-derived cell line (PDCL) of the recurrent GBM.

(B) Mutational signature of the patient's GBMs. Indicated is the frequency of variants in the primary and recurrent GBM after normalization to the patient's native genome. Note, the recurrent tumor shows a C>T mutational signature (TMZ signature) characteristic of hypermutated GBM after TMZ treatment.

(C) Venn diagram showing the sgRNA-ome of the patient's recurrent GBM, determined in both the patient's recurrent GBM tissue and in two technical replicates of the recurrent GBM PDCL. Numbers indicate cancer-specific sgRNAs, defined as those with at least one mismatch in the PAM-proximal eight nucleotides compared to the patient's native and reference genomes.

(D) Identification of mismatch location of cancer repeat sgRNAs when compared to the patient's native and reference genomes.

(E) Enrichment and depletion of sgRNAs from a CRISPR screen in NHA control and SF11411 PDCL cells. The sgRNAs were ranked based on the log(2) fold change (FC) of their representation from day 28 (D28) post transduction compared to day 1 (T0). Specific subsets of sgRNAs are highlighted.

(F) Quantification of cancer-specific sgRNA enrichment and depletion in NHA control versus SF11411 PDCL cells using MAGeCK RRA. Shown is the log(2)FC of normalized sgRNA representation between the two cell lines at the end of the screen (D28).

(G) Significantly depleted (FDR < 0.05, MAGeCK RRA gene level) sgRNAs enabling TMZ signature targeted cancer shredding. Note, cancer repeat sgRNAs showed the strongest cancer-specific depletion.

(H) Potential use cases of CRISPR cancer shredding. Targetable mutations include therapy-induced TMZ signature mutations. sgHYP, hypermutated cancer-specific sgRNAs. sgTMZ, TMZ signature mutations-specific sgRNAs. sgREC, recurrent cancer-specific sgRNAs.

KEY RESOURCES TABLE

REAGENT or RESOURCE	SOURCE	IDENTIFIER
Bacterial and virus strains		
Luciferase-IRES-mCherry lentivirus	GeneCopoeia	LPP-HLUC-Lv214-100-C
Endura ElectroCompetent cells	Lucigen	60242
Chemicals, peptides, and recombinant proteins		
Dulbecco's Modified Eagle Medium (DMEM)	Corning	10-013-CV
Fetal bovine serum (FBS)	Seradigm	1500-500
Penicillin-Streptomycin	Gibco	15140-122
Dulbecco's Modified Eagle Medium/Nutrient Mixture F-12 (DMEM/F-12)	Gibco	11320-033
Neurocult NS-A Basal Medium	Stemcell Technologies	05751
B27 Supplement minus vitamin A	Thermo Fisher Scientific	12587010
N2 Supplement	Thermo Fisher Scientific	17502001
GlutaMAX	Thermo Fisher Scientific	35050061
Sodium Pyruvate	Thermo Fisher Scientific	11360070
Recombinant Human EGF protein	Thermo Fisher Scientific	PHG0311
Recombinant Human FGF-Basic	PeproTech	100-18B
Laminin	Thermo Fisher Scientific	23017-015
Hoechst 33258	Polysciences	09460
4-Hydroxytamoxifen (4-OHT)	Sigma-Aldrich	H7904
Tamoxifen	Sigma-Aldrich	T5648-1G
Corn oil	Sigma-Aldrich	C8267
Polyethylenimine (PEI)	Polysciences	23966
Opti-MEM	Gibco	31985-070
Polybrene (Hexadimethrine bromide)	Sigma-Aldrich	H9268-5G
Puromycin	Invivogen	ant-pr-1
Hygromycin B	Thermo Fisher Scientific	10687010
Propidium iodide (PI)	Thermo Fisher Scientific	P3566
Temozolomide	Sigma-Aldrich	T2577
DMSO	Sigma-Aldrich	D2650
Crystal Violet Solution	Sigma-Aldrich	V5265
Critical commercial assays		
GenePrint 10 System	Promega	B9510
Comet Assay kit	Trevigen	4250-050-K
CellTiter-Glo Luminescent Cell Viability Assay	Promega	G7572
FxCycle PI/RNase Staining Solution	Invitrogen	F10797
Worthington Papain Dissociation System	Worthington	LK003150
Qiagen Plasmid Maxi Kit	Qiagen	12163
Quick-DNA Miniprep Plus Kit	Zymo Research	D4068

REAGENT or RESOURCE	SOURCE	IDENTIFIER
Deposited data		
CRISPR screen data	This paper	GEO: GSE244497
Experimental models: Cell lines		
HEK293T	Thermo Fisher Scientific	R70007; RRID:CVCL_6911
HEK-RT1	Oakes et al.[45]	N/A
DF-1	ATCC	CRL-12203; RRID:CVCL_0570
NHA-PC5	Ohba et al.[67]	N/A
NHA-N2	This paper	N/A
U-251	Sigma-Aldrich	09063001; RRID:CVCL_0021
LN-229	ATCC	CRL-2611; RRID:CVCL_0393
T98G	ATCC	CRL-1690; RRID:CVCL_0556
LN-18	ATCC	CRL-2610; RRID:CVCL_0392
SF11411	UCSF Brain Tumor Center Preclinical Therapeutics Core	N/A
GL261	UCSF Brain Tumor Center Preclinical Therapeutics Core	N/A
GBM12	Mayo Clinic Brain Tumor PDX national resource	N/A
GBM85	Mayo Clinic Brain Tumor PDX national resource	N/A
GBM123	Mayo Clinic Brain Tumor PDX national resource	N/A
Experimental models: Organisms/strains		
Female outbred athymic nude mice (*Foxn1*$^{nu/nu}$)	The Jackson Laboratory	007850
Oligonucleotides		
sgRNA sequences	Table S2	N/A
Pooled oligos for generating sgRNA library (sequences in Table S3)	Twist Bioscience	N/A
Primer-Amp_fw: cttgtggaaaggacgaaacaccg	IDT	N/A
Primer-Amp_rv: gctatgctgtttccagcatagctc	IDT	N/A
Primer-NGS_fw: ACACTCTTTCCCTACACGAC GCTCTTCCGATCTggactatcatatgcttaccg	IDT	N/A
Primer-NGS_rv: GTGACTGGAGTTCAGACGTGT GCTCTTCCGATCTggtgccacttttttcaagttg	IDT	N/A
Recombinant DNA		
pCF226-Cas9-Puro	Table S2	N/A
pCF287-TiCas9-P2A-Puro	Table S2	N/A
pCF820-sgRNA-mCherry2	Table S2	N/A
pCF821-sgRNA-mNeonGreen	Table S2	N/A

REAGENT or RESOURCE	SOURCE	IDENTIFIER
pCF822-sgRNA-Cas9-Puro	Table S2	N/A
pCF823-Cas9-Puro	Table S2	N/A
pCF826-sgRNA-Cas9-mCherry2	Table S2	N/A
pCF827-sgRNA-Cas9-mNeonGreen	Table S2	N/A
pCF525-AcrIIA4	Table S2	Addgene, #115795
psPAX2	Didier Trono Lab: Packaging and Envelope Plasmids (unpublished)	Addgene, #12260
pMD2.G	Didier Trono Lab: Packaging and Envelope Plasmids (unpublished)	Addgene, #12259
Software and algorithms		
FlowJo	BD Pharmingen	N/A
GraphPad Prism	GraphPad	N/A
ImageJ	NIH	N/A
MAGeCK	Li et al.[62]	N/A
SciPy (version 1.6.2)	https://scipy.org/	N/A
Circa (Version 1.2.2)	https://omgenomics.com/circa/	Maria Nattestad
BWA (Version 0.7.17)	https://bio-bwa.sourceforge.net/	Heng Li (lh3@sanger.ac.uk)
GATK (Version 3.8-1-0)	https://gatk.broadinstitute.org/hc/en-us	N/A
Jericho (Version 2.0)	Silico Therapeutics	N/A
GuideScan (Version 1.0)	Perez et al.[68]	N/A